

Comparative Studies of the Cellular Uptake, Subcellular Localization, and Cytotoxic and Phototoxic Antitumor Properties of Ruthenium(II)–Porphyrin Conjugates with Different Linkers

Jing-Xiang Zhang,^{†,‡} Jun-Wei Zhou,^{§,‡} Chi-Fai Chan,^{†,‡} Terrence Chi-Kong Lau,^{*,§} Daniel W. J. Kwong,[†] Hoi-Lam Tam,[‡] Nai-Ki Mak,^{||} Ka-Leung Wong,^{*,†} and Wai-Kwok Wong^{*,†}

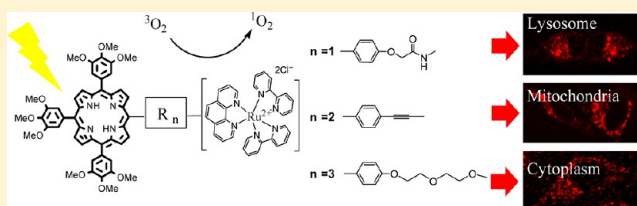
[†]Department of Chemistry, [‡]Department of Physics, and ^{||}Department of Biology, Hong Kong Baptist University, Kowloon Tong, Hong Kong SAR

[§]Department of Biology and Chemistry, City University of Hong Kong, Tat Chee Avenue, Kowloon Tong, Hong Kong SAR

Supporting Information

ABSTRACT: Six water-soluble free-base porphyrin-Ru(II) conjugates, 1–3, and Zn(II) porphyrin-Ru(II) conjugates, 4–6, with different linkers between the hydrophobic porphyrin moiety and the hydrophilic Ru(II)-polypyridyl complex, have been synthesized. The linear and two-photon-induced photophysical properties of these conjugates were measured and evaluated for their potential application as dual in vitro imaging and photodynamic therapeutic (PDT) agents.

Conjugates 1–3, with their high luminescence and singlet oxygen quantum yields, were selected for further study of their cellular uptake, subcellular localization, and cytotoxic and photocytotoxic (under linear and two-photon excitation) properties using HeLa cells. Conjugate 2, with its hydrophobic phenylethynyl linker, was shown to be highly promising for further development as a bifunctional probe for two-photon (NIR) induced PDT and in vitro imaging. Cellular uptake and subcellular localization properties were shown to be crucial to its PDT efficacy.



INTRODUCTION

Photodynamic therapy (PDT) has recently emerged as a promising alternative therapy against cancer, with several PDT agents approved and used clinically in the past two decades.^{1–3} In PDT, three key elements are required: a photosensitizer (PS), which when excited by light of an appropriate wavelength, converts molecular oxygen in tissues to the cytotoxic singlet oxygen (¹O₂).^{4–13} A porphyrin-based compound, shown to accumulate preferentially in solid tumors, was the first PDT agent approved by the U.S. Food and Drug Administration as a noninvasive antitumor treatment modality.^{14–16} Ruthenium and organoruthenium complexes have also been shown to be effective chemotherapeutic agents against a variety of cancer cells.^{17–21} Recently, several hydrophilic Ru(II)-porphyrin conjugates were synthesized and reported to have potent cytotoxic, as well as phototoxic activities toward tumors.^{22,23} The IC₅₀ values of these conjugates obtained under photoirradiation ($\lambda_{\text{irr}} = 590\text{--}700\text{ nm}$) were found to be lower by 1 order of magnitude than those obtained in the dark. However, the strongest absorptions of these Ru(II) conjugates were at ca. 420 nm, with less than 3% of their maximum absorption intensities found in the tissue-transparent region (>650 nm). To overcome this problem, we have designed some Ru(II)-porphyrin conjugates with substantial absorption under two-photon excitation at $\lambda_{\text{ex}} \geq 800\text{ nm}$.^{22–24} In these conjugates, the linkage of the Ru(II)-polypyridyl complex, a charge-transfer moiety, to the tetraphenylporphyrin raised its

two-photon absorption (TPA) cross section, σ^2 , from <20 GM to 178 GM, permitting their potential use as TPA-PDT agents against solid tumors. Furthermore, these conjugates became luminescent upon visible/near-infrared excitation in vitro, thus enabling their development as bifunctional tumor imaging and PDT agents.^{25,26} Nonetheless, to be an efficacious photochemotherapeutic agent, its cellular uptake and subcellular localization properties are important parameters to consider as well.²⁷

In this work, we report the synthesis of six amphiphilic Ru(II) appended porphyrins (1, 2, 3) and Zn(II) porphyrins (4, 5, 6) using linkers with different physicochemical (e.g., hydrophobic, electronic) properties and compare their luminescent (via linear and two-photon excitations), cellular uptake, subcellular localization, and (dark) cytotoxic and photocytotoxic properties in order to determine the optimal linker properties in these Ru(II)-porphyrin conjugates for TPA-PDT application.

EXPERIMENTAL SECTION (MATERIALS AND METHODS)

Synthesis of Compounds 1 to 6. All analytical-grade solvents were dried by standard procedures, distilled, and

Received: April 10, 2012

Revised: May 23, 2012

Published: July 9, 2012

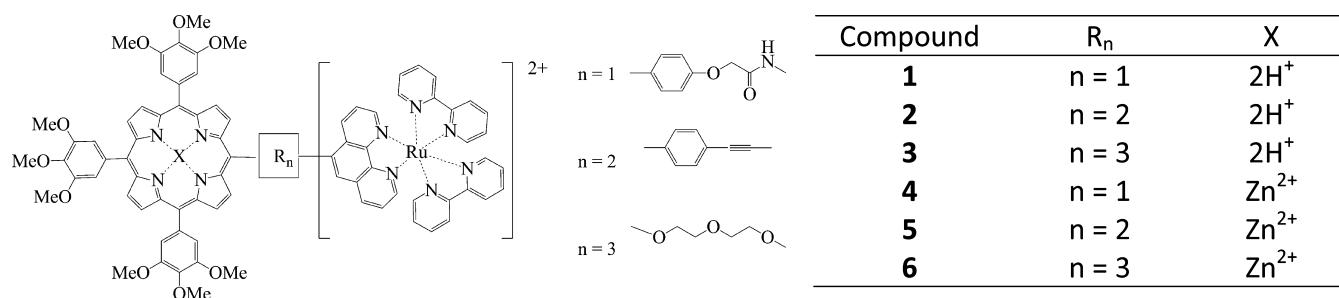
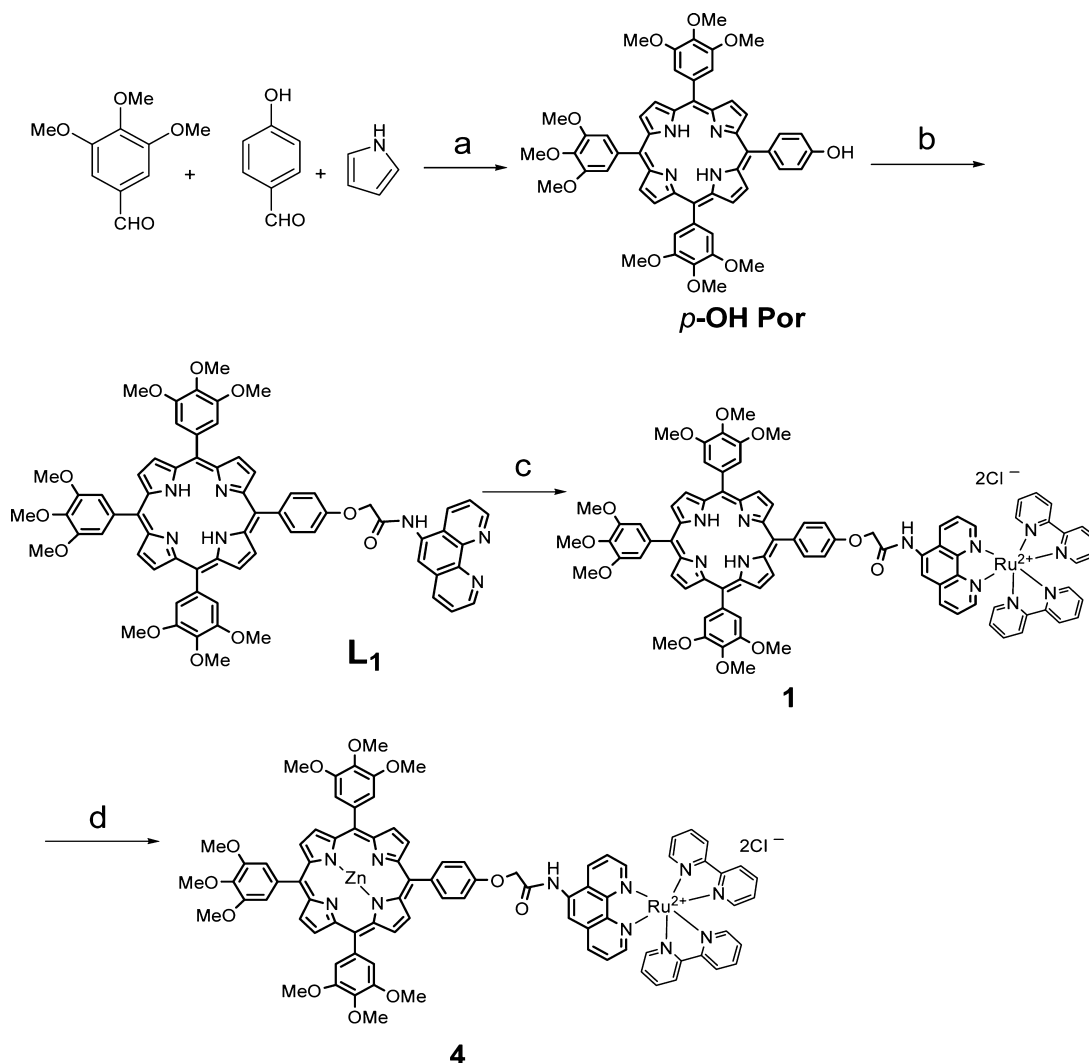


Figure 1. Schematic structures of ruthenium-porphyrin conjugates 1–6.

Scheme 1. Synthetic Route for Conjugates 1 and 4^a

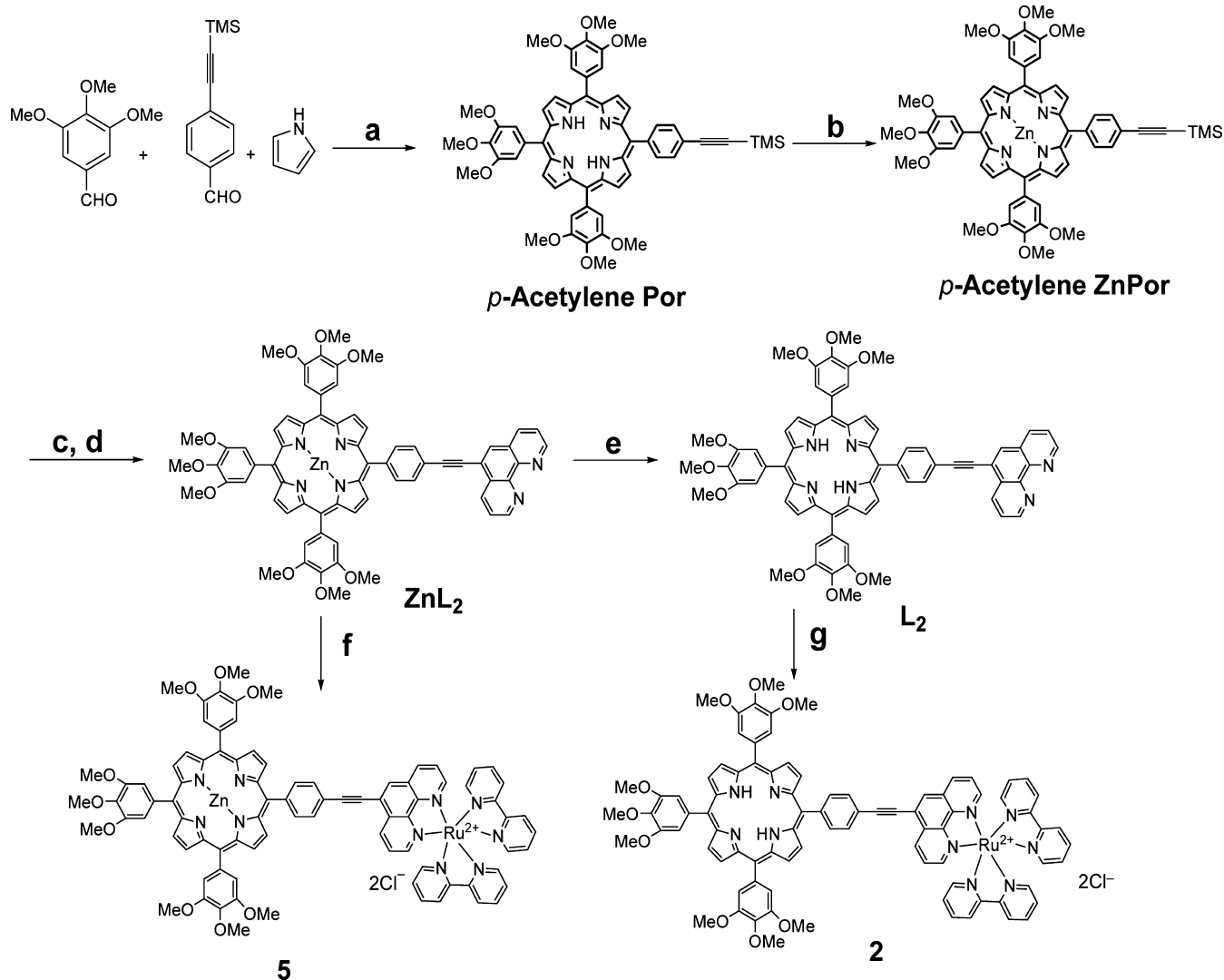


^aReactions and conditions: (a) propionic acid, 140 °C, 15%; (b) BrCH₂CONH-phen, Cs₂CO₃, DMF, 80 °C, 42%; (c) *cis*-Ru(bpy)₂Cl₂, THF/ethanol, 81%; (d) Zn(OAc)₂·2H₂O, MeOH, 98%.

deaired before use. NMR spectra were recorded on a Bruker Ultrashield 400 plus NMR spectrometer. The ¹H NMR chemical shifts were referenced to tetramethylsilane, TMS (*d* = 0.00). High-resolution mass spectra were obtained on a Bruker Autoflex MALDI–TOF mass spectrometer. IR spectra were recorded on Nicolet Magna 550 Series II. Preparations of *cis*-Ru(bpy)₂Cl₂,²⁸ 5-bromo-1,10-phenanthroline,²⁹ and di-(ethylene glycol) di-*p*-toluenesulfonate³⁰ were performed

according to literature procedures. The synthetic routes of compounds 1–6 are listed in Schemes 1, 2, and 3.

5,10,15-Tris(3',4',5'-trimethoxyphenyl)-20-(4'-hydroxyphenyl)-21H,23H-porphyrin (p-OH Por). A solution of pyrrole (4.556 g, 0.068 mol) in 100 mL of propionic acid was added dropwise into a solution of 3,4,5-trimethoxybenzaldehyde (10.00 g, 0.051 mol) and 4-hydroxybenzaldehyde (2.075 g, 0.017 mol) in 300 mL of propionic acid at 120 °C. When it is completed, the temperature was raised up to 140 °C. After

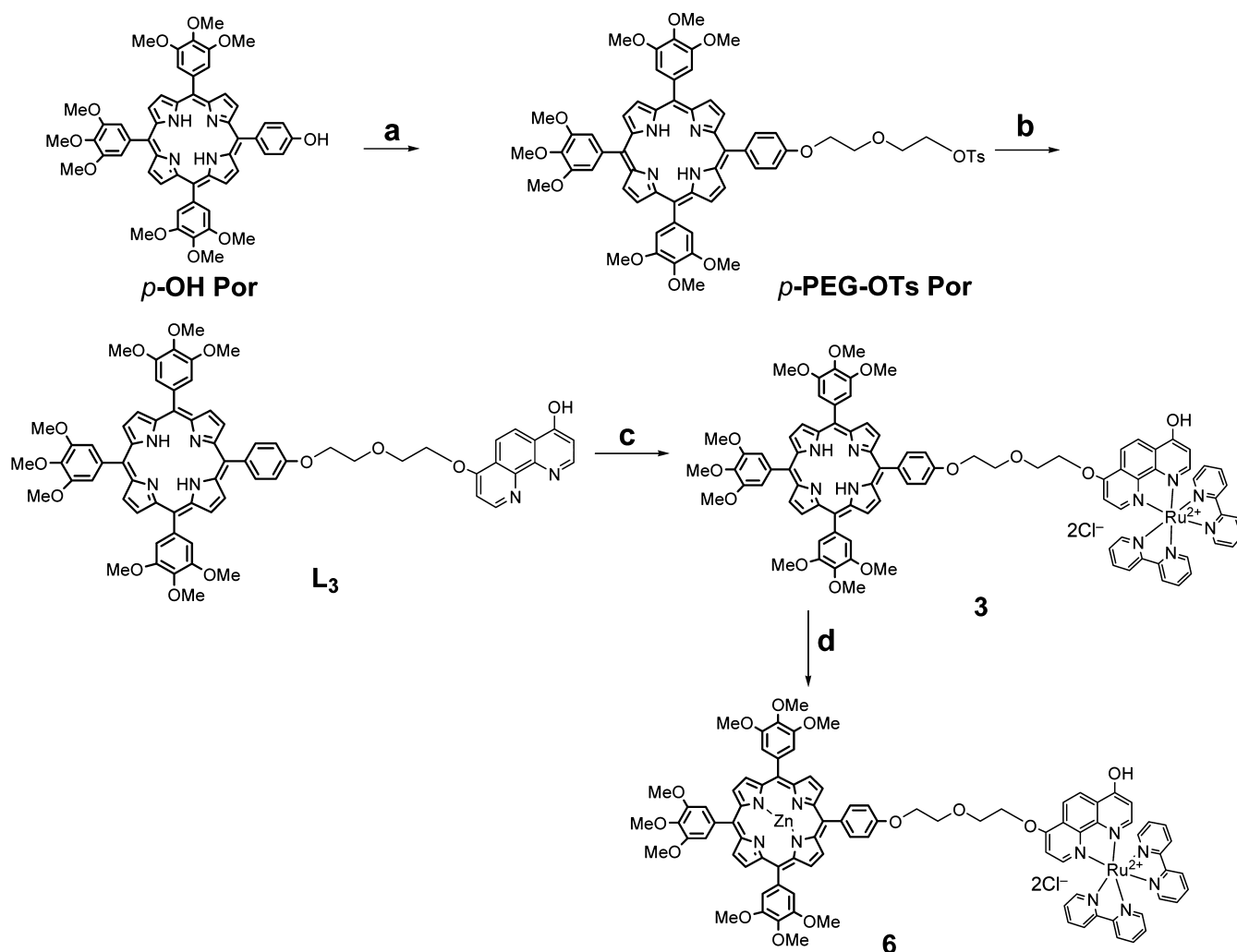
Scheme 2. Synthetic Route for Conjugates 2 and 5.^b

^bReactions and conditions: (a) propionic acid, 140 °C, 18%; (b) Zn(OAc)₂·2H₂O, CHCl₃, MeOH, 97%; (c) TBAF, THF; (d) Pd(PPh₃)₄, CuI, THF, diisopropylamine, 5-bromo-1,10-phen, 51% (two steps); (e) HCl, CH₂Cl₂, RT, 90%; (f) *cis*-Ru(bpy)₂Cl₂, THF/ethanol, 85%; (g) *cis*-Ru(bpy)₂Cl₂, THF/ethanol, 81%.

refluxing for 3 h, the propionic acid was distilled out under reduced pressure until about 80 mL solution was left. Then, 100 mL of ethanol was added into the flask and the solution was cooled overnight in the refrigerator. The precipitate was filtered out and washed with ethanol for several times. The product (2.297 g, 0.003 mol) was obtained in the second band as a purple solid after column chromatography (CHCl₃ as eluent), yield 15%. UV–visible (CHCl₃), λ_{abs}/nm (log ε) 422 (5.56), 518 (4.35), 553 (3.86), 592 (3.80), 648 (3.75). IR (KBr), ν/cm⁻¹: 2925 (s), 2847 (w), 1576 (s), 1495 (s), 1460 (s), 1401 (s), 1356 (s), 1245 (s), 1168 (m), 1119 (s), 996 (m), 972 (w), 918 (s), 792 (m), 730 (m), 587 (m). ¹H NMR (CDCl₃) δ -2.79 (s, 2H), 3.96 (s, 18H), 4.18 (s, 9H), 5.30 (s, 1H), 7.22 (d, 2H, J = 8.6 Hz), 7.46 (d, 6H, J = 1.6 Hz), 8.07 (d, 2H, J = 8.4 Hz), 8.88 (d, 2H, J = 4.7 Hz), 8.94 (d, 6H, J = 4.7 Hz). HRMS (MALDI-TOF) ([M]⁺, m/z): Calcd for C₅₃H₄₈N₄O₁₀, 900.9; Found for [M+H]⁺, 901.3.

Amide-Linked Porphyrin-Phen (L₁). 2-Bromo-*N*-(1,10-phenanthrolin-5-yl) acetamide (421 mg, 1.332 mmol) and Cs₂CO₃ (64 mg, 0.333 mmol) were added into a solution of *p*-OH Por

(200 mg, 0.222 mmol) in anhydrous DMF (10 mL). The solution was stirred for 24 h at 80 °C, and then the solvent was removed; the residue was extracted with CHCl₃ and washed with water. The organic solvent was collected and removed under reduced pressure. The crude product was purified by column chromatography (CHCl₃/MeOH (v/v) = 30:1); yield: 106 mg, 42%. UV–visible (CHCl₃), λ_{abs}/nm (log ε) 422 (5.51), 518 (4.30), 553 (3.87), 592 (3.70), 651 (3.68). IR (KBr), ν/cm⁻¹: 2917 (s), 2843 (w), 1699 (m), 1576 (s), 1499 (s), 1458 (s), 1401 (s), 1356 (m), 1233 (s), 1180 (m), 1119 (s), 1004 (m), 967 (w), 927 (m), 792 (s), 730 (m), 628 (w), 583 (w). ¹H NMR (CDCl₃) δ -2.76 (s, 2H), 3.98 (s, 18H), 4.19 (s, 9H), 5.16 (s, 2H), 7.48 (d, 6H, J = 2.0 Hz), 7.52 (d, 2H, J = 8.2 Hz), 7.69–7.72 (m, 1H), 7.80–7.84 (m, 1H), 8.27 (d, 2H, J = 8.4 Hz), 8.33–8.35 (dd, 1H, J = 1.6 Hz, 8.1 Hz), 8.44–8.46 (dd, 1H, J = 1.5 Hz, 8.4 Hz), 8.57 (s, 1H), 8.88 (d, 2H, J = 4.7 Hz), 8.98 (s, 6H), 9.14 (s, 1H), 9.20–9.22 (dd, 1H, J = 1.7 Hz, 4.4 Hz), 9.32 (dd, 1H, J = 1.7 Hz, 4.1 Hz). HRMS (MALDI-TOF) ([M]⁺): Calcd for C₆₇H₅₇N₇O₁₁, 1136.2; Found for [M]⁺, 1136.4.

Scheme 3. Synthetic Route for Conjugates 3 and 6^c

^cReactions and conditions: (a) Di(ethylene glycol) di-*p*-toluenesulfonate, K₂CO₃, DMF, 55%; (b) 4,7-diol-1,10-phen, NaH, DMF, 30%; (c) *cis*-Ru(bpy)₂Cl₂, acetic acid, reflux, 56%; (d) Zn(OAc)₂·2H₂O, MeOH, 88%.

Amide-Linked [(Porphyrin-Phen)Ru(bpy)₂][Cl]₂ (1). Porphyrin ligand L₁ (50 mg, 0.044 mmol) and *cis*-Ru(bpy)₂Cl₂ (85 mg, 0.176 mmol) were added into a solution of 15 mL THF and 15 mL ethanol, and then the solution was bubbled with N₂ for a few minutes, and the reaction temperature was set to 85 °C. After refluxing 15 h, the solvent was removed under vacuum and the residue was chromatographed on Al₂O₃ several times, the eluent in turn is CHCl₃, (CHCl₃:MeOH (v/v) = 12:1), yield 58 mg, 81%. UV-visible (CHCl₃), λ_{abs}/nm (log ε) 288 (4.91), 424 (5.58), 517 (4.29), 554 (3.98), 592 (3.79), 646 (3.65). IR (KBr), ν/cm⁻¹: 2925 (m), 2819 (w), 1580 (s), 1540 (m), 1499 (s), 1466 (s), 1405 (s), 1356 (m), 1233 (s), 1176 (m), 1119 (s), 1004 (m), 976 (m), 932 (m), 845 (w), 800 (m), 763 (m), 726 (m), 566 (m). ¹H NMR (d₆-DMSO) δ -2.91 (s, 2H), 3.89 (s, 18H), 3.99 (s, 9H), 5.39 (s, 2H), 7.36–7.40 (m, 2H), 7.50 (m, 8H), 7.58–7.62 (m, 4H), 7.84–7.89 (m, 3H), 7.94–7.98 (m, 1H), 8.06–8.14 (m, 3H), 8.16–8.23 (m, 5H), 8.78 (s, 1H), 8.82–8.91 (m, 7H), 8.94 (s, 6H), 9.18 (m, 1H), 11.31 (s, 1H). HRMS (MALDI-TOF) ([M-2Cl]⁺, *m/z*): Calcd for [C₈₇H₇₃N₁₁O₁₁Ru]⁺, 1549.6; Found for [M-2Cl]⁺, 1549.4.

Amide-Linked [(Zn-porphyrin-Phen)Ru(bpy)₂][Cl]₂ (4). 1 (30 mg, 0.0185 mmol) was treated with Zn(OAc)₂·2H₂O (5

mg, 0.022 mmol) in 20 mL of methanol at 65 °C for 3 h. The crude product was washed with water and then dried in vacuum. The pure product was obtained by flash chromatography on Al₂O₃, yield: 31 mg, 98%. UV-visible (CHCl₃), λ_{abs}/nm (log ε) 288 (4.94), 431 (5.67), 560 (4.28), 603 (4.32). IR (KBr), ν/cm⁻¹: 2917 (s), 2847 (w), 1593 (m), 1580 (s), 1540 (m), 1507 (s), 1458 (s), 1409 (s), 1343 (s), 1237 (s), 1176 (m), 1123 (s), 996 (m), 943 (m), 800 (m), 763 (m), 722 (m), 620 (m). ¹H NMR (d₆-DMSO) δ 3.90 (s, 18H), 4.00 (s, 9H), 5.33 (s, 2H), 7.35–7.38 (m, 2H), 7.43 (d, 6H, *J* = 6.2 Hz), 7.52 (d, 2H, *J* = 8.5 Hz), 7.58–7.63 (m, 4H), 7.83–7.88 (m, 3H), 7.94–7.99 (m, 1H), 8.06–8.15 (m, 5H), 8.19–8.24 (m, 3H), 8.75 (s, 1H), 8.79–8.87 (m, 7H), 8.89 (d, 6H, *J* = 4.4 Hz), 9.05 (d, 1H, *J* = 8.5 Hz), 11.06 (s, 1H). HRMS (MALDI-TOF) ([M-2Cl]⁺, *m/z*): Calcd for [C₈₇H₇₁N₁₁O₁₁RuZn]⁺, 1613.4; Found for [M-2Cl]⁺, 1612.1.

5,10,15-Tris(3',4',5'-trimethoxyphenyl)-20-[4'-(2''-trimethylsilylethyl)phenyl]-21H,23H-porphyrin (*p*-Acetylene Por). A solution of pyrrole (3.646 g, 0.054 mol) in propionic acid (100 mL) was added dropwise into a solution of 3,4,5-trimethoxybenzaldehyde (8.00 g, 0.041 mol) and 4-[2''-(trimethylsilyl)ethynyl]benzaldehyde (2.748 g, 0.014 mol) in propionic acid (300 mL) at 120 °C. When it was completed,

the temperature was raised up to 140 °C. After refluxing for 3 h, the propionic acid was distilled out completely under reduced pressure. The residue was dissolved in CHCl₃ and filtered through a short silica gel column and then the filtrate was washed with water. The crude product was purified by column chromatography using CHCl₃ as eluent. Purple solid was obtained. Yield: 2.400 g, 18%. UV–visible (CHCl₃), $\lambda_{\text{abs}}/\text{nm}$ (log ϵ) 422 (5.65), 516 (4.31), 553 (3.90), 591 (3.83), 648 (3.81). IR (KBr), ν/cm^{-1} : 2925 (s), 2823 (m), 1576 (s), 1499 (s), 1470 (s), 1405 (s), 1352 (s), 1225 (s), 1176 (m), 1123 (s), 1017 (m), 967 (w), 918 (m), 861 (m), 792 (m), 730 (m), 653 (w), 567 (w). ¹H NMR (CDCl₃) δ –2.80 (s, 2H), 0.38 (s, 9H), 9.36 (s, 18H), 4.18 (s, 9H), 7.45 (s, 6H), 7.86 (d, 2H, J = 8.2 Hz), 8.16 (d, 2H, J = 8.3 Hz), 8.91 (d, 2H, J = 4.7 Hz), 9.08 (m, 6H). HRMS (MALDI-TOF) ($[M]^+$, m/z): Calcd for C₅₈H₅₆N₄O₉Si, 981.2; Found for $[M]^+$, 981.2.

5,10,15-Tris(3',4',5'-trimethoxyphenyl)-20-[4'-[2''-(trimethylsilyl)ethynyl]-phenyl]-21H,23H porphyrinato zinc(III) (p-Acetylene ZnPor). Zn(OAc)₂·2H₂O (107 mg, 0.490 mmol) and porphyrin **p-Acetylene Por** (400 mg, 0.408 mmol) were dissolved in a mixture of CHCl₃ and MeOH, and the reaction was maintained at 60 °C for 3 h. The solvent was removed and the residue was purified on a silica gel using CHCl₃ as eluent to give **7** as purple solid. Yield: 413 mg, 97%. ¹H NMR (CDCl₃) 0.39 (s, 9H), δ 3.92 (s, 18H), 4.12 (s, 9H), 7.45 (s, 6H), 7.86 (d, 2H, J = 8.1 Hz), 8.07 (d, 2H, J = 8.0 Hz), 8.93 (d, 2H, J = 4.7 Hz), 9.07 (m, 6H).

Phenylacetylene-Linked Zinc-Porphyrin-Phen (ZnL₂). **p-Acetylene ZnPor** (380 mg, 0.364 mmol) was dissolved in anhydrous CH₂Cl₂ in N₂ atmosphere, TBAF solution (400 μ L, 1 M in THF) was injected into the CH₂Cl₂ solution and the resultant solution was stirred at room temperature for 30 min. The reaction solution was filtered by flash chromatography and the deprotected ethynyl-zinc-porphyrin was dried in vacuum. 5-Bromo-1,10-phenanthroline (62.8 mg, 0.242 mmol) and then 20 mL of anhydrous THF was added in the above flask. The Sonogashira coupling reaction was administered in N₂ atmosphere using Pd(PPh₃)₄ (28 mg, 0.024 mmol) and CuI (2.3 mg, 0.012 mmol) as catalysts and diisopropylamine (6 mL) as base. The reaction mixture was heated at 45 °C for 8 h. The solvent was removed and the residue was purified on silica gel using CHCl₃/MeOH (v/v = 20:1) as eluent, yield 142 mg, 51%. UV–visible (CHCl₃), $\lambda_{\text{abs}}/\text{nm}$ (log ϵ) 278 (4.20), 426 (5.58), 553 (4.30), 595 (3.95). IR (KBr), ν/cm^{-1} : 2921 (s), 2851 (w), 1617 (s), 1576 (s), 1556 (m), 1535 (w), 1503 (s), 1458 (s), 1405 (s), 1348 (s), 1237 (s), 1127 (s), 992 (m), 935 (w), 796 (m), 718 (m), 669 (m), 567 (s). ¹H NMR (CDCl₃) δ 3.97 (s, 18H), 4.19 (s, 9H), 7.49 (d, 6H, J = 1.7 Hz), 7.68–7.71 (m, 1H), 7.81–7.88 (m, 1H), 8.08 (d, 2H, J = 8.1 Hz), 8.27 (s, 1H), 8.29–8.31 (m, 3H), 8.97 (d, 2H, J = 4.7 Hz), 9.04–9.08 (m, 7H), 9.18 (d, 1H, J = 3.6 Hz), 9.25 (d, 1H, J = 2.8 Hz). HRMS (MALDI-TOF) ($[M]^+$, m/z): Calcd for C₆₇H₅₂N₆O₉Zn, 1148.3; Found for $[M+H]^+$, 1149.3.

Phenylacetylene-Linked Porphyrin-Phen (L₂). Demetalation of ZnL₂ was achieved by dissolving ZnL₂ (60 mg, 0.052 mmol) in a mixture of concentrated HCl (2 mL) and CH₂Cl₂ (10 mL). After stirring for 1 h, the solvent was washed by water and the organic phase was neutralized by NaHCO₃. The solvent was dried by sodium sulfate and removed under reduced vacuum. Purification was done on silica gel to give purple–red solid of L₂. Yield: 51 mg, 90%. UV–visible (CHCl₃), $\lambda_{\text{abs}}/\text{nm}$ (log ϵ) 282 (4.18), 424 (5.57), 518 (4.27), 554 (3.83), 592 (3.83), 648 (3.76). IR (KBr), ν/cm^{-1} : 2913 (s), 2855 (w), 1638 (s), 1613

(s), 1580 (s), 1511 (m), 1454 (m), 1405 (w), 1356 (m), 1241 (s), 1119 (s), 1070 (w), 1004 (w), 927 (s), 804 (m), 726 (w), 665 (w), 575 (w). ¹H NMR (CDCl₃) δ –2.75 (s, 2H), 3.98 (d, 18H, J = 4.2 Hz), 4.18 (d, 9H, J = 4.2 Hz), 7.49 (m, 6H), 7.69 (m, 1H), 7.84 (m, 1H), 8.10 (m, 2H), 8.27 (d, 1H, J = 3.4 Hz), 8.30 (m, 3H), 8.91 (d, 2H, J = 4.4 Hz), 8.99–9.06 (m, 7H), 9.22–9.26 (m, 1H), 9.29–9.33 (m, 1H). HRMS (MALDI-TOF) ($[M]^+$, m/z): Calcd for C₆₇H₅₄N₆O₉, 1086.4; Found for $[M+H]^+$, 1087.4.

Phenylacetylene-Linked [(Zinc-Porphyrin-Phen)Ru(bpy)₂][Cl]₂ (5). Zinc-porphyrin ligand ZnL₂ (50 mg, 0.044 mmol) and cis-Ru(bpy)₂Cl₂ (63 mg, 0.131 mmol) were added in a mixture of THF (15 mL) and ethanol (15 mL). The solution was then bubbled with N₂ for a few minutes, and heated to 85 °C. After refluxing 15 h, the solvent was removed under vacuum and the residue was chromatographed on Al₂O₃ several times, and the eluent in turn was CHCl₃, (CHCl₃:MeOH (v/v) = 12:1). Yield: 60 mg, 85%. UV–visible (CHCl₃), $\lambda_{\text{abs}}/\text{nm}$ (log ϵ) 288 (4.92), 431 (5.55), 562 (4.46), 606 (4.31). IR (KBr), ν/cm^{-1} : 2921 (s), 2843 (w), 1625 (s), 1572 (s), 1482 (m), 1462 (s), 1405 (s), 1348 (s), 1229 (s), 1115 (s), 1061 (w), 988 (s), 935 (m), 792 (w), 763 (m), 722 (m), 543 (m). ¹H NMR (d₆-DMSO) δ 3.91 (d, 18H, J = 11.7 Hz), 4.06 (d, 9H, J = 10.6 Hz), 7.37–7.40 (m, 2H), 7.51 (d, 6H, J = 4.8 Hz), 7.57–7.61 (m, 2H), 7.74–7.79 (m, 4H), 7.83–7.87 (m, 1H), 7.91 (d, 2H, J = 7.2 Hz), 7.95–7.99 (m, 3H), 8.08–8.12 (m, 2H), 8.18–8.24 (m, 3H), 8.31 (d, 1H, J = 5.1 Hz), 8.61 (s, 1H), 8.65–8.68 (m, 3H), 8.73–8.79 (m, 4H), 8.89 (d, 2H, J = 4.7 Hz), 8.94–8.97 (m, 4H), 9.15 (d, 1H, J = 8.4 Hz). HRMS (MALDI-TOF) ($[M-2Cl]^+$, m/z): Calcd for C₈₇H₆₈N₁₀O₉RuZn, 1563.9; Found for $[M-2Cl]^+$, 1563.2; $[M-2Cl-bpy]^+$, 1408.1.

Phenylacetylene-Linked [(Porphyrin-Phen)Ru(bpy)₂][Cl]₂ (2). Porphyrin ligand L₂ (50 mg, 0.046 mmol) and cis-Ru(bpy)₂Cl₂ (67 mg, 0.138 mmol) were dissolved in a mixture of THF (15 mL) and ethanol (15 mL). The solution was then bubbled with N₂ for a few minutes before heating to 85 °C. After refluxing 15 h, the solvent was removed under vacuum and the residue was chromatographed on Al₂O₃ several times; the eluent in turn was CHCl₃ (CHCl₃:MeOH (v/v) = 12:1). Yield: 58 mg, 81%. UV–visible (CHCl₃), $\lambda_{\text{abs}}/\text{nm}$ (log ϵ) 288 (4.66), 425 (5.33), 517 (4.12), 554 (3.91), 593 (3.72), 646 (3.66). IR (KBr), ν/cm^{-1} : 2925 (s), 2843 (w), 1643 (s), 1609 (s), 1576 (w), 1503 (m), 1450 (m), 1405 (s), 1380 (m), 1237 (w), 1119 (s), 993 (m), 800 (m), 767 (w), 661 (w), 561 (m). ¹H NMR (d₆-DMSO) δ –2.98 (s, 2H), 3.82 (s, 18H), 3.91 (s, 9H), 7.32–7.37 (m, 2H), 7.45 (d, 6H, J = 7.8 Hz), 7.54–7.57 (m, 2H), 7.61 (d, 2H, J = 5.4 Hz), 7.80 (s, 2H), 7.88–7.91 (m, 1H), 7.99–8.03 (m, 1H), 8.06–8.11 (m, 2H), 8.13–8.21 (m, 6H), 8.31 (d, 2H, J = 8.0 Hz), 8.81–8.93 (m, 14H), 9.21 (d, 1H, J = 8.6 Hz). HRMS (MALDI-TOF) ($[M-2Cl]^+$, m/z): Calcd for C₈₇H₇₀N₁₀O₉Ru, 1500.6; Found for $[M-2Cl]^+$, 1500.4; $[M-2Cl+DHB]^+$, 1653.0.

1-[4-[5,10,15-Tris(3,4,5-trimethoxyphenyl)-20-porphyrinyl]-phenoxy]-5-(p-tolylsulfonyloxy)ethoxy-ethane (p-PEG-OTs Por). Di(ethylene glycol) di-p-toluenesulfonate (345 mg, 0.832 mmol) and porphyrin **p-OH Por** (300 mg, 0.332 mmol) were dissolved in anhydrous DMF (10 mL), and then K₂CO₃ (68 mg, 0.498 mmol) was added into the solution. The reaction solution was heated at 65 °C for 24 h. DMF was removed and the residue was washed with water several times and extracted with CH₂Cl₂. The organic phase was collected and purified on silica gel to give **p-PEG-OTs Por** as purple solid. Yield: 208 mg, 55%. UV–visible (CHCl₃), $\lambda_{\text{abs}}/\text{nm}$ (log ϵ) 422 (5.68), 518

(4.41), 553 (3.87), 592 (3.87), 648 (3.80). IR (KBr), ν/cm^{-1} : 2921 (s), 2847 (w), 1707 (s), 1646 (w), 1597 (s), 1580 (s), 1495 (s), 1462 (m), 1413 (s), 1352 (s), 1327 (s), 1233 (s), 1172 (s), 1131 (s), 1000 (m), 923 (m), 812 (m), 763 (m), 661 (m), 555 (m). ^1H NMR (CDCl_3) δ -2.78 (s, 2H), 2.45 (s, 3H), 3.92 (m, 2H), 3.97 (s, 18H), 4.15 (m, 2H), 4.17 (s, 9H), 4.31 (m, 2H), 4.37 (m, 2H), 7.30 (d, 2H, $J = 8.7$ Hz), 7.47 (d, 6H, $J = 1.5$ Hz), 7.78 (d, 2H, $J = 8.3$ Hz), 7.86 (d, 2H, $J = 8.3$ Hz), 8.11 (d, 2H, $J = 8.4$ Hz), 8.87 (d, 2H, $J = 4.7$ Hz), 8.94 (d, 6H, $J = 5.3$ Hz). HRMS (MALDI-TOF) ($[\text{M}]^+$, m/z): Calcd for $\text{C}_{64}\text{H}_{62}\text{N}_4\text{O}_{14}\text{S}$, 1143.2; Found for $[\text{M}]^+$, 1143.4.

Ethoxyethane-Linked Porphyrin-Phen (L_3). 1,10-Phenanthroline-4,7-diol (74 mg, 0.350 mmol) was dissolved in 5 mL anhydrous DMF, and then NaH (17 mg, 0.7 mmol) was added to the solution. The solution was stirred for 20 min, then a DMF solution of porphyrin *p*-PEG-OTs Por (200 mg, 0.175 mmol) was added dropwise into the reaction mixture. The reaction temperature was maintained at 50 °C for 8 h. DMF was removed and CH_2Cl_2 was added. The unreacted 1,10-phenanthroline-4,7-diol was filtered out and the organic phase was washed by water for several times. The product was purified on silica gel with the mixed solvent ($\text{CHCl}_3/\text{MeOH}$ (v/v) = 25:1) as eluent. Yield: 62 mg, 30%. UV-visible (CHCl_3), $\lambda_{\text{abs}}/\text{nm}$ (log ϵ) 330 (4.30), 422 (5.72), 516 (4.43), 554 (3.89), 591 (3.88), 648 (3.80). IR (KBr), ν/cm^{-1} : 2917 (s), 2847 (w), 1625 (m), 1580 (s), 1499 (s), 1458 (s), 1405 (s), 1352 (m), 1303 (w), 1282 (w), 1233 (s), 1168 (m), 1119 (s), 1049 (m), 1004 (m), 967 (m), 914 (w), 792 (s), 628 (w), 555 (m). ^1H NMR (CDCl_3) δ -2.78 (s, 2H), 3.96 (s, 18H), 4.18 (s, 9H), 4.21 (m, 2H), 4.27 (m, 2H), 4.48 (m, 2H), 4.54 (m, 2H), 6.48 (d, 1H, $J = 7.3$ Hz), 7.03 (d, 1H, $J = 5.2$ Hz), 7.29 (d, 2H, $J = 8.5$ Hz), 7.46 (s, 6H), 7.73 (m, 1H), 8.08–8.14 (m, 3H), 8.37 (d, 1H, $J = 9.0$ Hz), 8.75 (d, 1H, $J = 5.2$ Hz), 8.84 (d, 2H, $J = 4.6$ Hz), 8.92–8.95 (m, 6H), 10.41 (s, 1H). HRMS (MALDI-TOF) ($[\text{M}]^+$, m/z): Calcd for $\text{C}_{69}\text{H}_{62}\text{N}_6\text{O}_{13}$, 1183.2; Found for $[\text{M}]^+$, 1183.4.

Ethoxyethane-Linked [(Porphyrin-(5-hydroxyl-Phen)Ru(bpy) $_2$)] $[\text{Cl}]_2$ (3). Porphyrin ligand L_3 (50 mg, 0.042 mmol) and cis-Ru(bpy) $_2\text{Cl}_2$ (61 mg, 0.127 mmol) were added to acetic acid (10 mL). Then, the reaction solution was refluxed under N_2 atmosphere for 3 h. The solvent was removed under vacuum and the residue was chromatographed on Al_2O_3 several times; the eluents in turn were ($\text{CHCl}_3/\text{MeOH}$ (v/v) = 20:1), ($\text{CHCl}_3/\text{MeOH}$ (v/v) = 10:1). Yield: 39 mg, 56%. UV-visible (CHCl_3), $\lambda_{\text{abs}}/\text{nm}$ (log ϵ) 288 (4.71), 424 (5.48), 517 (4.30), 554 (3.98), 592 (3.97), 646 (3.71). IR (KBr), ν/cm^{-1} : 2921 (s), 2847 (m), 1629 (s), 1576 (m), 1508 (m), 1462 (s), 1404 (s), 1343 (m), 1282 (w), 1231 (s), 1131 (s), 1119 (s), 1053 (m), 1010 (m), 955 (w), 759 (s), 628 (w), 555 (m). ^1H NMR (d_6 -DMSO) δ -2.92 (s, 2H), 3.89 (d, 18H, $J = 2.0$ Hz), 3.99 (d, 9H, $J = 2.6$ Hz), 4.09–4.12 (m, 4H), 4.44–4.51 (m, 4H), 6.14 (d, 1H, $J = 6.8$ Hz), 6.74 (d, 1H, $J = 6.8$ Hz), 7.26 (d, 1H, $J = 6.3$ Hz), 7.37–7.45 (m, 5H), 7.47–7.51 (m, 8H), 7.58 (d, 1H, $J = 6.1$ Hz), 7.77 (d, 1H, $J = 5.7$ Hz), 7.81–7.84 (m, 2H), 7.87–7.91 (m, 2H), 7.96–8.03 (m, 2H), 8.05–8.12 (m, 4H), 8.27–8.30 (m, 1H), 8.70–8.80 (m, 6H), 8.93–8.96 (m, 6H). HRMS (MALDI-TOF) ($[\text{M}-2\text{Cl}]^+$, m/z): Calcd for $\text{C}_{89}\text{H}_{78}\text{N}_{10}\text{O}_{13}\text{Ru}$, 1596.7; Found for $[\text{M}-2\text{Cl}]^+$, 1596.4.

Ethoxyethane-Linked [(Zn-porphyrin-(5-hydroxyl-Phen))-Ru(bpy) $_2$] $[\text{Cl}]_2$ (6). Ethoxyethane-linked [(porphyrin-(5-hydroxyl-Phen))Ru(bpy) $_2$] $[\text{Cl}]_2$ (3) (18 mg, 0.011 mmol) was treated with $\text{Zn}(\text{OAc})_2 \cdot 2\text{H}_2\text{O}$ (3 mg, 0.013 mmol) in methanol (20 mL) at 65 °C for 3 h. The crude product was washed with

water and then dried under vacuum. The pure product was obtained by column chromatography on Al_2O_3 ($\text{CHCl}_3/\text{MeOH}$ (v/v) = 10:1 as eluent). Yield: 16 mg, 88%. UV-visible (CHCl_3), $\lambda_{\text{abs}}/\text{nm}$ (log ϵ) 288 (4.72), 431 (5.64), 562 (4.28), 600 (4.01). IR (KBr), ν/cm^{-1} : 2921 (s), 2847 (w), 1625 (s), 1576 (m), 1503 (m), 1454 (s), 1405 (s), 1343 (m), 1282 (w), 1229 (s), 1131 (s), 1119 (s), 1053 (m), 1004 (m), 967 (w), 759 (s), 628 (w), 555 (m). ^1H NMR (d_6 -DMSO) δ 3.83 (d, 18H, $J = 2.5$ Hz), 3.93 (d, 9H, $J = 2.2$ Hz), 4.03–4.07 (m, 4H), 4.39–4.46 (m, 4H), 6.00 (d, 1H, $J = 6.8$ Hz), 6.64 (d, 1H, $J = 6.8$ Hz), 7.24 (d, 1H, $J = 6.4$ Hz), 7.28–7.35 (m, 3H), 7.36–7.39 (m, 7H), 7.42–7.46 (m, 3H), 7.52 (d, 1H, $J = 6.2$ Hz), 7.72 (d, 1H, $J = 5.8$ Hz), 7.76–7.78 (m, 2H), 7.80–7.83 (m, 2H), 7.93–7.98 (m, 4H), 8.01–8.06 (m, 2H), 8.14 (d, 1H, $J = 9.0$ Hz), 8.68–8.76 (m, 6H), 8.83–8.86 (m, 6H). HRMS (MALDI-TOF) ($[\text{M}-2\text{Cl}]^+$, m/z): Calcd for $[\text{C}_{89}\text{H}_{76}\text{N}_{10}\text{O}_{13}\text{RuZn}]^+$, 1660.1; Found for $[\text{M}-2\text{Cl}-\text{H}]^+$, 1658.9.

Linear-Induced Photophysical Properties. UV-visible absorption spectra in the spectral range 200–1100 nm were recorded by an HP UV-8453 spectrophotometer. Single-photon luminescence spectra were recorded using an Edinburgh Instrument FLS920 combined fluorescence lifetime and steady state spectrophotometer that was equipped with a visible to near-infrared-sensitive photomultiplier by in-nitrogen flow-cooled housing. The spectra were corrected for detector response and stray background light phosphorescence. The emission quantum yields of all the compounds were measured by a demountable 142 mm (inner) diameter barium sulfide-coated integrating sphere supplied with two access ports in Edinburgh Instrument FLS920. pH titrations of porphyrin-Ru homometallic complexes 1–3 were performed on 10 μM (DMSO) samples dissolved in aqueous solution whose pH was adjusted by small addition of 1 M NaOH or HCl.

Two-Photon Induced Emission and Two-Photon Absorption Cross-Section Measurement. Two-photon absorption spectra of 1–6 were measured at 850 nm by the open-aperture Z-scan method³¹ using 100 fs laser pulses with a peak power of 276 GW cm^{-2} from an optical parametric amplifier operating at a 1 kHz repetition rate generated from a Ti:Sapphire regenerative amplifier system. The laser beam was split into two parts by a beam splitter. One was monitored by a photodiode (D1) as the incident intensity reference, I_0 , and the other beam was detected by the photodiode (D2) as the transmitted intensity. After passing through a lens with $f = 20$ cm, the laser beam was focused and passed through a quartz cell. The position of the sample cell, z , was moved along the laser-beam direction (z axis) by a computer-controlled translatable table so that the local power density within the sample cell could be changed under the constant incident intensity laser power level. Finally, the transmitted intensity from the sample cell was detected by the photodiode D2 interfaced to a computer for signal acquisition and averaging. Each transmitted intensity data represent an average of over 100 measurements. Assuming a Gaussian beam profile, the nonlinear absorption coefficient β can be obtained by curve fitting to the observed open-aperture traces, $T(z)$, with eq 1

$$T(z) = 1 - \frac{\beta I_0 (1 - e^{-\alpha_0 L})}{2a_0 [1 + (z/z_0)^2]} \quad (1)$$

where a_0 is the linear absorption coefficient, l is the sample length (1 mm quartz cell), and z_0 is the diffraction length of the incident beam.

After obtaining the nonlinear absorption coefficient β , the two-photon absorption cross section σ_2 of the sample molecule (in units of GM, where 1 GM = 10^{-50} cm⁴ s photon⁻¹) can be calculated using eq 2

$$\sigma_2 = \frac{1000\beta h\nu}{N_A d} \quad (2)$$

where N_A is the Avogadro constant, d is the concentration of the sample compound in solution, h is the Planck constant, and ν is the frequency of the incident laser beam.

Singlet Oxygen Quantum Yield Measurement. Singlet oxygen was detected directly by its phosphorescence emission at 1270 nm using an InGaAs detector on a PTI QM4 luminescence spectrometer. The singlet oxygen quantum yields (Φ_Δ) of the test compounds were determined in CHCl₃ by comparing the singlet oxygen emission intensity of the sample solution to that of a reference compound (H₂TPP, $\Phi_\Delta = 0.55$ in CHCl₃)³² according to eq 3³³

$$\Phi_\Delta^S = \Phi_\Delta^{\text{REF}} \times \left(\frac{n_S}{n_{\text{REF}}} \right)^2 \frac{G_\Delta^S}{G_\Delta^{\text{REF}}} \times \frac{A_{\text{REF}}}{A_S} \quad (3)$$

where Φ_Δ is the singlet oxygen quantum yield, G_Δ is the integrated emission intensity, A is the absorbance at the excitation wavelength, n is the refractive index of the solvent. Superscripts REF and S correspond to the reference and the sample, respectively. In all measurements, the ¹O₂ emission spectra were obtained using an excitation with the absorbance set at 0.05 in order to minimize reabsorption of the emitted light.

Cell Culture. Human cervical carcinoma (HeLa) cells were maintained in an RPMI 1640 medium supplemented with 10% fetal bovine serum (FBS) and 1% penicillin and streptomycin in 5% CO₂. Culture medium in each dish was changed prior to exposure to the test compounds. Stock solutions of the test compounds (1 mM) were prepared in aqueous solution and stored in the dark at room temperature. These compounds, when used in the imaging and bioassay experiments involving cultured cells, were diluted with the corresponding culture media to appropriate concentrations.

Confocal Microscopic Imaging of Compounds 1–6. HeLa cells (1×10^5) were seeded onto coverslip in 35 mm culture dishes for overnight. The cells were initially incubated with compounds 1–6 (1 μ M) for 30 min in the dark. For colocalization experiments, the cells were then washed and stained with 100 nM mitochondria-specific probe Mito Tracker Green FM dye M7514 or lysosome-specific probe Lyso Tracker Green DND-26 L7526, for 30 min. The emitted fluorescent signals of tested compounds and the organelle-specific probes were examined using the Leica SP5 (upright configuration) confocal microscope equipped with argon laser, HeCd laser and a femtosecond-pulsed Ti:Sapphire laser (Libra II, Coherent) inside the tissue culture chamber (5% CO₂, 37 °C). A 40 \times oil immersion objective and pinhole size of 110 μ m was used for image capturing.

Flow Cytometric Cellular Uptake. HeLa cells (10^5 per sample) were seeded to 35 mm Petri dish for overnight and then the cells were incubated with drugs at 2 mM for 1 and 6 h. Cells were trypsinized and washed with PBS for twice. The drug's uptakes by the HeLa cells were analyzed with flow

cytometry. The cells were excited with 488 nm argon laser and emission was collected with FL-3 (equipped with 650 nm long pass filter) and 10000 events were analyzed.

Photocytotoxicity Assay. HeLa cells (2×10^4 /well) were incubated in wells of a 96-well plate overnight. The cells were treated with 1, 2, and 3 for 6 h in the dark. The culture medium was then replaced with fresh medium and the cells were exposed to yellow light (1–4 J/cm²) produced from a 400 W tungsten lamp fitted with a heat-isolation filter and a 500 nm long-pass filter. The fluence rate was 4 mW/cm². Cell viability was determined by the MTT reduction assay at 24 h post-PDT.³⁴ The cell monolayers were rinsed twice with phosphate-buffered saline (PBS) and then incubated with 250 μ g/mL MTT solution at 37 °C for 3 h. The formazan crystal formed was dissolved in DMSO and the absorbance of dissolved formazan crystal at 540 and 690 nm was measured using a 96-well plate reader (ELx800 Absorbance Microplate Reader).

Two-Photon-Induced Confocal Microscopic Imaging of 1–3. HeLa cells (1×10^5) were seeded onto coverslip in 35-mm culture dishes overnight. The cells were initially incubated with 1–3 for 6 h in the dark. The two-photon-induced fluorescent signals of 1–3 were captured using the Leica SP5 (upright configuration) confocal microscope equipped with a femtosecond-pulsed Ti:Sapphire laser (Libra II, Coherent) inside the tissue culture chamber (5% CO₂, 37 °C). The excitation beam produced by the femtosecond laser, which was tunable from 680 to 1050 nm, was focused on the adherent cells through a 40 \times oil immersion objective. For the evaluation of effectiveness of photodynamic therapy, the time-lapse images (0–32 min, one laser shot per 8 min) were obtained with femtosecond laser excitation at 850 nm (laser power \sim 8 mW).

RESULTS AND DISCUSSION

Synthesis and Characterization. (Scheme 1) The substitution reaction of 2-bromo-*N*-(1,10-phenanthroline-5-yl)-acetamide and 5,10,15-tris(3,4,5-trimethoxyphenyl)-20-(4-hydroxyphenyl)-21*H*,23*H*-porphyrin (*p*-OH Por) in the presence of Cs₂CO₃ in DMF afforded the L₁ porphyrin ligand with a yield of 42%. The identity of L₁ was confirmed by ¹H NMR, in which the two internal NH pyrrole protons appeared as a sharp singlet at ca. –2.7 ppm, the two CH₂ protons appeared as a singlet at ca. 5.1 ppm, the seven protons of 1,10-phenanthroline occurred at ca. 8.2–8.5 ppm (4 protons) and 9.1–9.5 ppm (3 protons), respectively. High-resolution mass spectrum of L₁ showed two peaks at m/z 1136.4, which corresponded to the peak [M+H]⁺ (cf. calculated [M]⁺, m/z 1135.4) and m/z 901, which corresponded to the loss of the 2-bromo-*N*-(1,10-phenanthroline-5-yl)acetamide fragment. Ru(II) complexation was carried out with cis-Ru(bpy)₂Cl₂ in mixed solvent THF/CH₃CH₂OH (1:1), giving compound 1 with 81% yield. Metalation of the porphyrin in 1 with zinc acetate afforded compound 4 in good yield. Both 1 and 4 were characterized by ¹H NMR, HRMS, IR, and UV–vis spectroscopies. In their ¹H NMR spectra (Figure S1 and S3), the two internal NH pyrrole protons of 1 appeared as a relatively broad singlet at –2.9 ppm and the bipyridine protons in both 1 and 4 appeared as multiplets in the downfield region. The high-resolution mass spectra of 1 and 4 are given in Figures S2 and S4, respectively. Figure S2 shows a single peak at m/z 1549.4, which corresponds to the molecular ion peak of 1 (calculated [M]⁺, m/z 1549.6), and Figure S4 shows a single peak at m/z 1612.1, which corresponds to the loss of a proton in either the pyrrole ring or the amide bond of 4 (calculated [M]⁺, m/z 1613.4).

In Scheme 2, Sonogashira coupling reaction between *p*-acetylene-ZnP_{or} and 5-bromo-1,10-phenanthroline under N₂ atmosphere afforded the zinc porphyrin, ZnL₂, in moderate yield. Demetalation of ZnL₂ in concentrated HCl solution gave the free base porphyrin, L₂. ¹H NMR spectra of L₂ and ZnL₂ show the Phen proton signals at δ ≈ 8.2–8.4 ppm (4 protons) and 9.2–9.5 ppm (3 protons), respectively. High-resolution mass spectra of L₂ and ZnL₂ show their respective [M+H]⁺ peaks at *m/z* 1087.4 (calculated [M]⁺, *m/z* 1086.4) and *m/z* 1149.3 (calculated [M]⁺, *m/z* 1148.3). Reaction of L₂ and ZnL₂ with *cis*-Ru(bpy)₂Cl₂ gave conjugates 2 and 5, respectively, in good yields. These products were characterized by ¹H NMR, HRMS, IR, and UV–vis spectra. The ¹H NMR spectra (in *d*₆-DMSO) of 2 displayed slightly broader peaks and overlapping resonances for the bipyridine protons can be observed in the region 8.0–8.5 ppm. The two internal pyrrole NH protons also located in the upfield region (δ = –2.9 ppm). High-resolution mass spectrum of 2 shows two peaks at *m/z* 1500.4 (M⁺) and 1653.3 ([M+DHB]⁺). ¹H NMR spectrum of 5 has a relatively well-resolved pattern, possibly because of its more symmetric structure. High-resolution mass spectrum of 5 also shows two peaks, one at *m/z* 1563.2 (M⁺) and the other at *m/z* 1408.1 ([M-bipyridine]⁺).

In Scheme 3, the reaction between *p*-OH Por and diethylene glycol di-*p*-toluenesulfonate in 1:1 ratio gave *p*-PEG-OTs Por as the main product. Reaction of *p*-PEG-OTs Por with 4,7-di-1,10-phenanthroline in the ratio of 1:2 gave L₃ with a relatively low yield, owing to the poor solubility of 4,7-di-1,10-phenanthroline in the reaction media. The complexation of L₃ with *cis*-Ru(bpy)₂Cl₂ gave 3, which upon metalation with Zn(OAc)₂ afforded 6. These final products, 3 and 6, were also characterized by ¹H NMR, HRMS, IR, and UV–vis spectroscopies. ¹H NMR spectra of 3 and 6 are quite similar with well-resolved peaks. High-resolution mass spectra of both 3 and 6 show single peaks at *m/z* 1596.4 and 1658.9, which match favorably to the calculated *m/z* values of their respective molecular ions (for 3, calculated [M]⁺, *m/z* 1596.7; and for 6, calculated [M]⁺, *m/z* 1660.1).

Photophysical Properties. The objective of this work is to develop a dual probe capable of *in vitro* imaging and photodynamic therapeutic treatment. Herein, we report the relevant photophysical properties, which include both the linear and multiphoton-induced photophysical properties, singlet oxygen quantum yields, and so forth, of the porphyrin-Ru(II) conjugates synthesized.

UV–visible Absorption. The UV–vis absorption spectra of the six conjugates (1 to 6) were recorded in DMSO. Figure 2 shows the electronic spectra of free-base porphyrin-Ru(II) conjugates 1 to 3, with the intense π to π* transitions, the Soret band, and the four weak Q-bands of the porphyrin found at ~300 nm, ~430 nm, and 500–700 nm, respectively. Introduction of a Zn(II) ion to the porphyrin in conjugates 4 to 6, resulted in small (a few nm) red shift of the Soret band and the number of Q bands were reduced from four to two.³⁵

Linear (One-Photon) Emission Spectra. The emission spectra of the six Ru(II)-porphyrin conjugates, excited at 430 nm and measured in DMSO, are shown in Figure 3. The free-base porphyrin-Ru(II) conjugates, 1, 2, and 3, show intense emission bands at ~655 and ~718 nm (Figure 3, upper panel). These two bands are assigned to the Q(0–0) and Q(0–1) transitions of the free-base porphyrins based on their emission wavelengths and lifetimes. The emission quantum yields of these conjugates, measured relative to the reference standard of

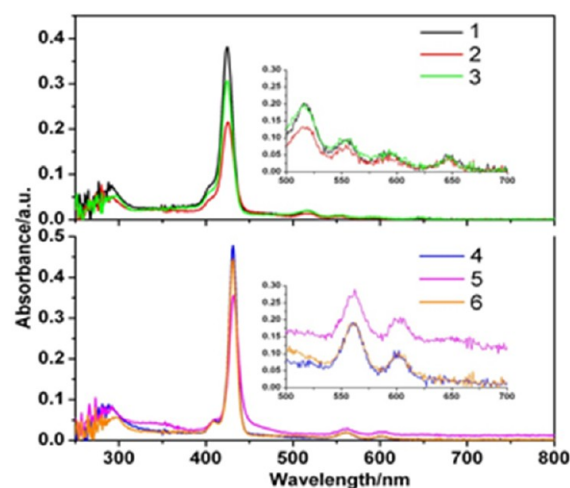


Figure 2. UV–vis absorption spectra of conjugates 1–3 (upper) and 4–6 (lower) in DMSO (1 μM). The inset shows the Q bands between 500 and 700 nm.

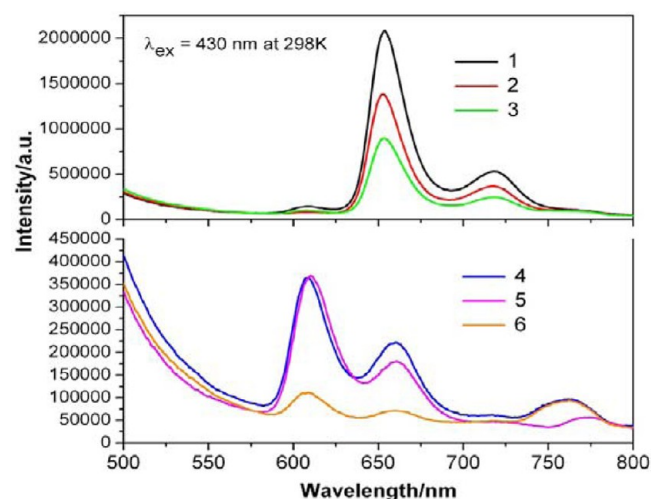


Figure 3. Emission spectra (λ_{ex} = 430 nm) of 1 μM of 1–3 (upper panel) and 4–6 (lower panel) measured in DMSO at 298 K.

5,10,15,20-tetrakis(4-methoxyphenyl)porphyrin,³⁶ are given in Table 1. From this table, it can be seen that the emission quantum yields of conjugates 1, 2, and 3 are strongly influenced by the length and conjugation of the linker between the porphyrin moiety and the Ru(bpy)₂(phen)²⁺ complex. By elongating the linkage using an ethoxyethane group in 3, we observed a dramatic reduction in the emission quantum yields from 5.30% (1) and 4.96% (2) to 1.93% (3). This result indicates that the observed porphyrin emissions are due to an energy transfer from the excited Ru(II)-polypyridyl moiety (λ_{abs}^{max} ≈ 450 nm) to the porphyrin.

The Ru(II)–Zn(II) porphyrin conjugates, 4, 5, and 6, give emission peaks at 610, 659, and 760 nm (Figure 3, lower panel) with the first two peaks assigned to the fluorescent emissions of the Zn(II) porphyrin. The 760 nm peak was assigned to the phosphorescence of the Zn(II) porphyrin.³⁷ The significant reduction in emission intensity observed in 6 is due to the longer ethoxyethane linkage between Ru(phen)(bpy)₂²⁺ and Zn(II) porphyrin, making energy transfer between these two chromophores less efficient.

Table 1. Photophysical Properties of the Ru(II)-Porphyrin Conjugates 1 to 6

compound	$\lambda_{\text{Abs}}/\text{nm}$ (log ϵ)	emission/nm (τ/ns)	$\Phi_{\text{em}}^a/\%$	$\Phi_{\Delta}^b/\%$	σ/GM
1	288(4.91), 424(5.58), 517(4.29), 554(3.98), 592(3.79), 646(3.65)	607(weak) 655(10.70), 718(8.78)	5.30	43	177
2	288(4.66), 425(5.33), 517(4.12), 554(3.91), 593 (3.72), 646(3.66)	607(weak) 654(11.6), 718(9.54)	4.90	58	168
3	288(4.71), 424(5.48), 517(4.30), 554(3.98), 592(3.97), 646(3.71)	607(weak) 653(4.23), 718(3.82)	1.93	38	144
4	288(4.94), 431(5.67), 560(4.28), 603(4.32)	610(10.50), 659(3.88) 760(weak)	0.58	52	172
5	288(4.92), 431(5.55), 562(4.46), 606(4.31)	610(3.74), 659(3.06) 760(weak)	0.30	73	228
6	288(4.72), 431(5.64), 562(4.28), 600(4.01)	610(3.04), 659(3.50) 770(weak)	0.16	45	106

^aThe emission quantum yields of 1 to 6 ($\lambda_{\text{em}} = 550\text{--}800\text{ nm}$, $\lambda_{\text{ex}} = 430\text{ nm}$). ^bThe $^1\text{O}_2$ quantum yields of 1 to 6 ($\lambda_{\text{ex}} = 430\text{ nm}$). ^cTwo-photon absorption cross sections of 1 to 6 ($\text{GM} = 10^{-50}\text{ cm}^4\text{ s photon}^{-1}\text{ molecule}^{-1}$, $\lambda_{\text{ex}} = 800\text{ nm}$), with an average measurement uncertainty of $\pm 23.5\text{ GM}$.

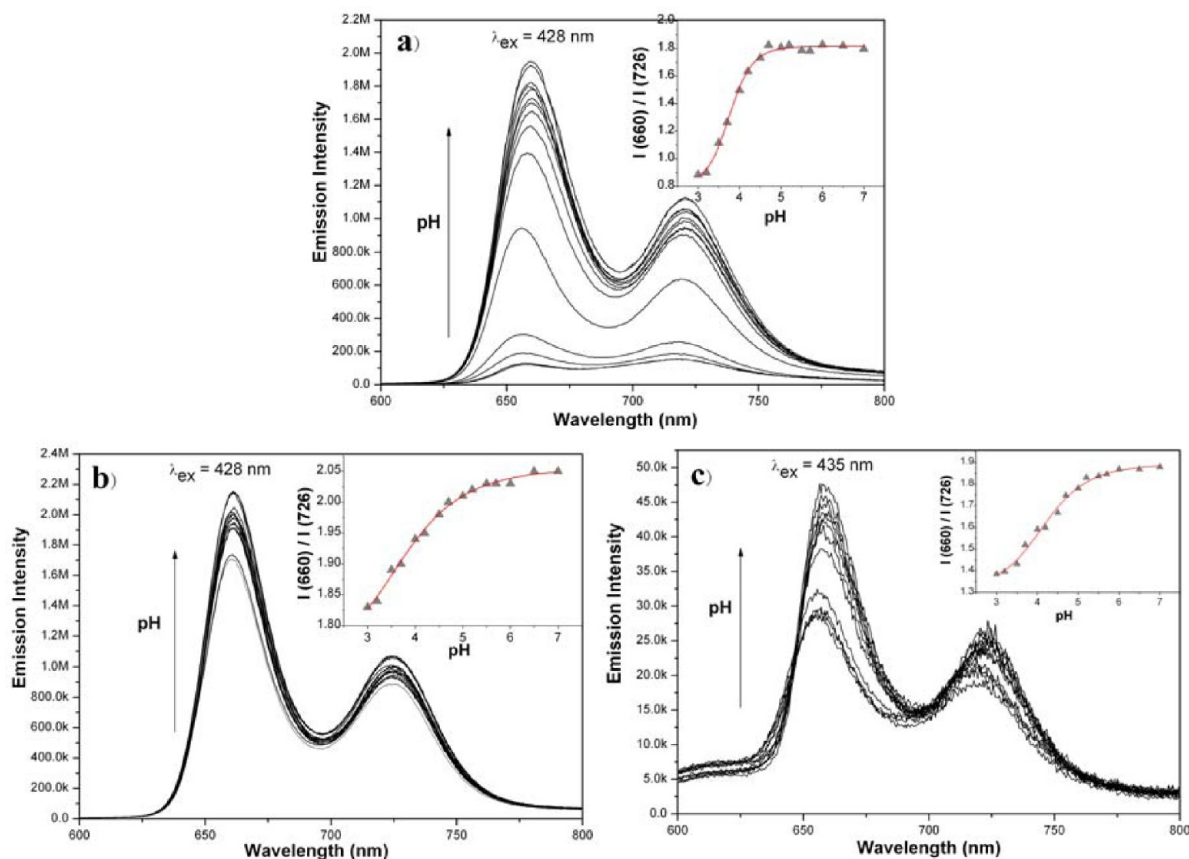


Figure 4. Emission spectral response of 10 μM of free-base porphyrin-Ru(II) conjugates 1 (a), 2 (b), and 3 (c) as a function of pH (pH = 3–7) measured in aqueous solution (295 K, <5% DMSO, $\lambda_{\text{ex}} = 428\text{ nm}$ for 1 and 2, 435 nm for 3). Inset: Variation of the intensity ratio of the emission at 659 and 718 nm of 1–3 with pH in aqueous solution. The data were fitted with a sigmoidal function (shown as red curves) to give the following apparent pK_a values: 3.75 (7) for 1, 3.26 (8) for 2, and 4.39 (0) for 3.

The emission spectra of the free-base porphyrin-Ru(II) (1, 2, and 3) and the Zn(II) porphyrin-Ru(II) (4, 5, and 6) series of conjugates are seen to be quite similar to those of the Ru(bpy)₂-(pyridylporphyrin)₂ hybrid (1:2) complexes synthesized and studied by Kon et al.³⁷ These authors showed that the excitation energy transfer mechanism in the Ru(II)-porphyrin conjugates corresponded to an energy transfer from the excited Ru(II) ¹MLCT state via its ³MLCT state to the porphyrin B₁ singlet state. However, in Zn(II) porphyrin, the energy level of the porphyrin singlet state becomes destabilized, as shown by a blue shift of ca. 45 nm ($\sim 1126\text{ cm}^{-1}$), resulting in the porphyrin singlet state of these conjugates being higher in energy than the Ru(II) ³MLCT excited state. This led to a reverse energy transfer in conjugates 4–6, where the energy migrates from the Soret-excited porphyrin to the Ru(II) chromophore. Even though this is not the first example of

reverse energy transfer going from free-base porphyrin-Ru(II) to Zn(II) porphyrin-Ru(II) conjugates, the emission quantum yield variations among these two systems are obviously different compared to other systems in the literature.^{38–40}

pH-Dependence Emission Change. It is well-known that the cellular uptake of an acidic organelle probe used to stain lysosomes as well as other acidic subcellular compartments, such as trans-Golgi vesicles, endosomes, and so forth,^{41–45} is driven by the plasma membrane H⁺ gradient.^{46–48} Free-base porphyrin (H₂P), with two imine nitrogens which can be protonated at low pH to give the mono-(H₃P⁺) and dication (H₄P²⁺), can potentially serve as an in vitro probe for the subcellular acidic organelles and compartments.

In principle, two distinct protonation reactions can occur on a free-base porphyrin, but the proton affinity of this macrocycle is generally represented by an averaged protonation constant,

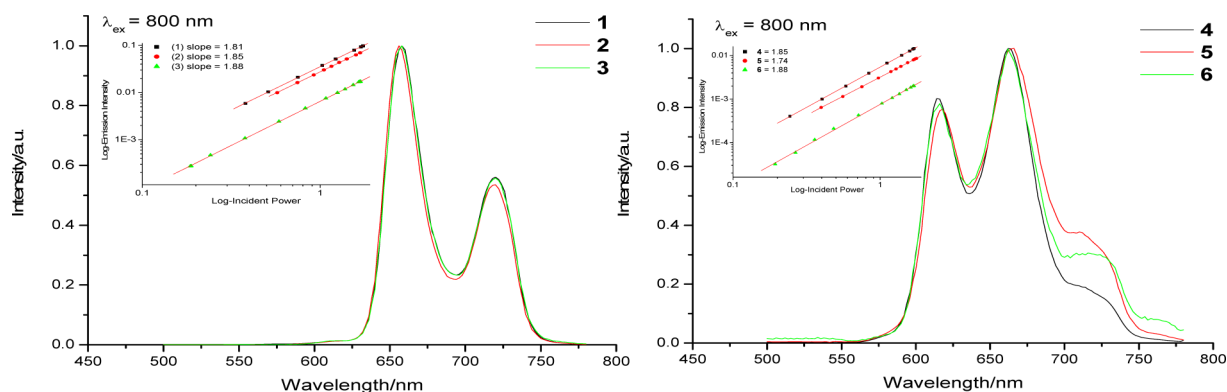


Figure 5. The two-photon induced emission spectra of conjugates 1–3 (left) and 4–6 (right) in aqueous DMSO (10 μ M, $\lambda_{\text{ex}} = 800$ nm). Inset: Plots of the observed emission intensities (1–3, $\lambda_{\text{em}} = 650$ nm; 4–6, $\lambda_{\text{em}} = 610$ nm) against the laser excitation ($\lambda_{\text{ex}} = 800$ nm) power used.

pK, as often only one pK value can be determined in pH titration experiments. The pK values measured for most water-soluble porphyrins were in the range 2–4⁴⁹ and were shown to depend on a complex interplay of the following factors: electronic effects of the substituents, the degrees of planarity and extended conjugation,^{50–52} and the peripheral charges, which provide electrostatic shielding to the protonation site, surrounding the porphyrin.^{53,54} In this work, we attempted to evaluate the potential application of the free-base porphyrin-Ru(II) conjugates, 1–3, as probes for subcellular acidic compartments by studying their spectral changes under different pH conditions and measure their pK values.

Absorption spectra of the deprotonated (free-base) form of 1–3 in aqueous solution (pH = 10.0) showed their Soret bands at ~ 428 nm (Figure S13) and the characteristic four-band pattern in the Q-band region, which is typical for tetraarylporphyrins. At pH 2, the fully protonated form of 1–3 (i.e., porphyrin dication) exhibited a red-shifted Soret band ($\lambda_{\text{max}} \approx 450$ nm) with increased intensity and a single Q-band pattern ($\lambda_{\text{max}} \approx 665$ nm) due to the higher symmetry of the porphyrin dication. The fluorescence spectra of 1–3 (Figure S14) also show clear changes upon protonation. The emission spectra of these free-base porphyrins show two well-defined peaks, a strong emission at 660 nm and a weak emission at 726 nm at pH 10. However, when fully protonated at pH 2 (i.e., dicationic form), only one broad emission band at around 715 nm was seen.

Figure 4 shows the emission spectral changes of the conjugates 1–3 in the pH range 3.0–7.0. The change in the fluorescence intensity ratio at 660 and 726 nm (I_{660}/I_{726}) for 1–3 from pH 3.0 to 7.0 is shown as insets in Figure 4 as well. The fluorescence intensity of these conjugates at 660 nm increases with increasing pH, corresponding to the conversion of the porphyrin from its dicationic form to the free-base form. Fitting the I_{660}/I_{726} vs pH curve (insets, Figure 4) with a Sigmoidal function of the Hasselbach equation⁵⁵ gave the following protonation constants pK for these conjugates: ~ 3.75 (1), ~ 3.26 (2), and ~ 4.39 (3). At first glance, the relatively lower pK values in 1 and 2 can be explained in terms of the more extensive π -conjugation in these conjugates with conjugative linkers which decreases the porphyrin pK via delocalization of the core electron density and reduces the intrinsic basicity of the macrocycle.⁵⁰ However, the perpendicular orientation adopted by the phenyl ring in the linkers of 1 and 2 relative to the porphyrin ring does not seem to support a significant extension of π -conjugation beyond the macrocycle

(vide infra). Thus, at this point we have no adequate explanation for the significantly lower pK values observed in 1 and 2 as compared to 3.

¹O₂ Quantum Yield. To assess their potential application as PDT agents, the ¹O₂ production yields of these Ru(II)-porphyrin conjugates were measured based on the phosphorescence intensities of the ¹O₂ produced upon photoirradiation (at 430 nm) of these compounds. Figure S15 shows the ¹O₂ phosphorescence spectra of the Ru(II)-porphyrin conjugates, 1–6, together with tetraphenylporphyrin, H₂TTP, used as a reference, in CHCl₃. On the basis of the ¹O₂ quantum yield of H₂TTP ($\Phi_{\Delta} = 0.55 \pm 0.11$),³⁵ the relative Φ_{Δ} values of these conjugates are given in Table 1. Conjugates 2 and 5, with their relative Φ_{Δ} estimated to be 0.58 ± 0.11 and 0.73 ± 0.11 , respectively, exhibited the highest ¹O₂ yields in their respective series of free-base and Zn(II) porphyrin-Ru(II) conjugates. A comparison of the trend of ¹O₂ quantum yields with that of the emission quantum yields for the two series of conjugates (1–3 and 4–6) shows no apparent correlation, suggesting that the energy transfer pathways leading to emission and ¹O₂ production are perhaps distinct. A more detailed investigation of these photophysical processes by transient absorption spectroscopy will be undertaken.

Two-Photon Induced Emission and Absorption. Photoexcitation in the near-infrared (NIR) region followed by luminescence at a shorter wavelength in the visible region is known as NIR-induced visible emission. This is a rather unusual process because apparently low-energy photons are “converted” to higher energy photons. This process is accomplished by the simultaneous absorption of two or three NIR photons via virtual intermediate states to produce a real excited state, which then returns to the ground state by the emission of a single photon in the visible region. The study of two- or three-photon induced emission processes on novel organic materials has received considerable attention recently because of potential applications in bioimaging and photodynamic therapy, optical data storage, and microfabrication.^{56–58}

Figure 5 shows the emission spectra of a series of Ru(II)-porphyrin conjugates, 1–6, in aqueous DMSO (0.4 mM) excited by near-infrared femtosecond laser ($\lambda_{\text{ex}} = 800$ nm). The emission spectral profiles (i.e., band shape, position, and width) obtained bear a close resemblance to the corresponding single-photon emission spectra (shown in Figure 3) of these conjugates. To confirm the involvement of two photons in the observed induced emission, the emission peak intensities of these conjugates were plotted against the incident laser

excitation power at 800 nm (inset of Figure 5). A slope of 1 in this plot would indicate that the emission resulted from one-photon absorption, whereas a slope of 2 is indicative of a two-photon absorption process. The slopes obtained for these conjugates in these plots (1.81 for 1, 1.88 for 2, 1.85 for 3, 1.87 for 4, 1.88 for 5, 1.83 for 6) clearly demonstrate the two-photon nature of their induced emissions.

Open-aperture Z-scan method ($\lambda_{\text{ex}} = 800 \text{ nm}$) was used to measure their two-photon absorption properties of conjugates 1–6. The Z-scan traces and the derived two-photon absorption cross sections, σ^2 (average uncertainty $\pm 23.5 \text{ GM}$), of these conjugates are shown in Figure 6 and Table 1, respectively.

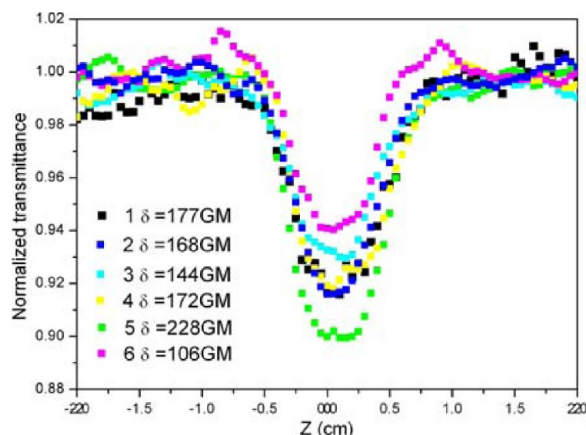


Figure 6. Open-aperture Z-scan traces of 0.4 mM of free-base porphyrin-Ru conjugates (1–3) and Zn(II) porphyrin-Ru conjugates (4–6) excited at 800 nm in DMSO. The average power of the laser beam was 0.271 mW.

The σ^2 value measured for conjugate 1 ($177 \pm 23.5 \text{ GM}$) was found to be virtually identical to that of a structurally very similar Ru(II)-porphyrin conjugate, Ru-P ($178 \pm 26.8 \text{ GM}$),²⁵ indicating that hydrophobic perturbation of the porphyrin substituent (3,4,5-trimethoxyphenyl in 1 vs phenyl in Ru-P) exerts no effect on the two-photon absorption cross section of these conjugates. Since σ^2 is strongly dependent on the π -conjugation length of a molecule, the lack of substantial enhancement in the σ^2 of conjugates 1 and 2 relative to 3 must be due to the perpendicular orientation of their *meso*-substituted phenyl linkers with respect to the porphyrin ring, which does not support extending the porphyrin π -conjugation to the polypyridyl ligand of the Ru(II) complex via the ethynyl

and amide linkages. This interpretation is consistent with the substantially higher σ^2 value (555 GM) observed in a similar free-base porphyrin-Ru(phen)(bpy)₂²⁺ conjugate connected through a β -ethynyl only linkage (i.e., no intervening phenyl ring).⁵²

In Vitro Studies. On the basis of the observed photophysical properties (i.e., stronger emission and ¹O₂ quantum efficiency) of the Ru(II)-porphyrin conjugates studied, the free-base porphyrin-Ru(II) conjugates, 1, 2, and 3, appear to be more suitable for further investigation as potential dual probes for imaging and photodynamic therapy. The following in vitro experiments, i.e., flow cytometry for cellular uptake, MTT assay for cytotoxicity (dark and light), subcellular localization imaging, and two-photon PDT experiments, were carried out to evaluate the potential biological and clinical applications of these compounds.

Cellular Uptake. In the past decades, many luminescent transition metal complexes have been extensively studied for potential in vitro and in vivo applications. However, most research work have been devoted to the screening of these complexes for biological applications, with few studies focusing on the effects of a systematic variation of particular structural elements on particular in vitro and/or in vivo properties of these complexes.^{60–62} Puckett et al.⁶³ measured and compared the cellular uptake, a crucial property for any bioprobe and drug molecule, of Ru(II) complexes with different polypyridyl ligands by human cervical carcinoma HeLa cells and investigated the underlying transport mechanism as well.⁴² In this work, we examined the cellular uptake properties of these porphyrin-Ru(II) conjugates with different linkers by HeLa cells using flow cytometry. The results obtained are shown in Figure 7.

From Figure 7, conjugates 1 and 2, with relatively hydrophobic linkers between the porphyrin and the Ru(II)-polypyridyl complex, are seen to be taken up by the HeLa cells much more efficiently than conjugate 3, which contains a relatively more hydrophilic ethoxyethane linker. For 3, the luminescence signal observed, which was indicative of the number of 3-loaded cells, after 6 h of incubation, was even less than those observed after 1 h of incubation with 1 and 2. Thus, even taking into account that 3 is ca. 2–3-fold less luminescent (i.e., lower Φ_{em}) than 1 and 2, the data support the following order of cellular uptake rates: 1 ~ 2 \gg 3.

Subcellular Localization. Localization of these porphyrin-Ru(II) conjugates ($2 \mu\text{M}$) within the HeLa cells after incubation for 6 h was examined by laser confocal microscopy

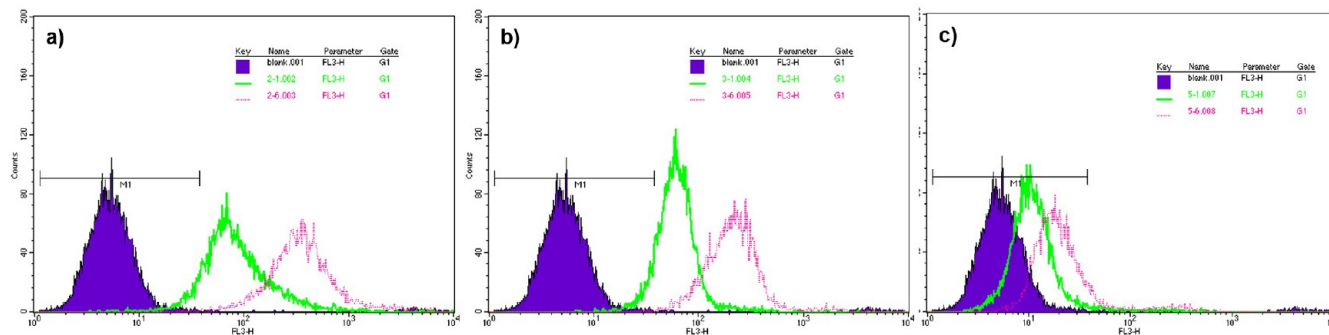


Figure 7. Flow cytometric analysis of the cellular uptakes of $2 \mu\text{M}$ of 1 (a), 2 (b), and 3 (c) by HeLa cells (10^5 cells per sample) after incubation for 1 h (green curve) and 6 h (pink curve) in dark. The luminescence signal ($\lambda_{\text{ex}} = 488 \text{ nm}$) was collected using FL-2 channels equipped with a long pass filter ($>650 \text{ nm}$). At least 10 000 events were counted. Live cells were differentiated by their low To-Pro-3 emission.

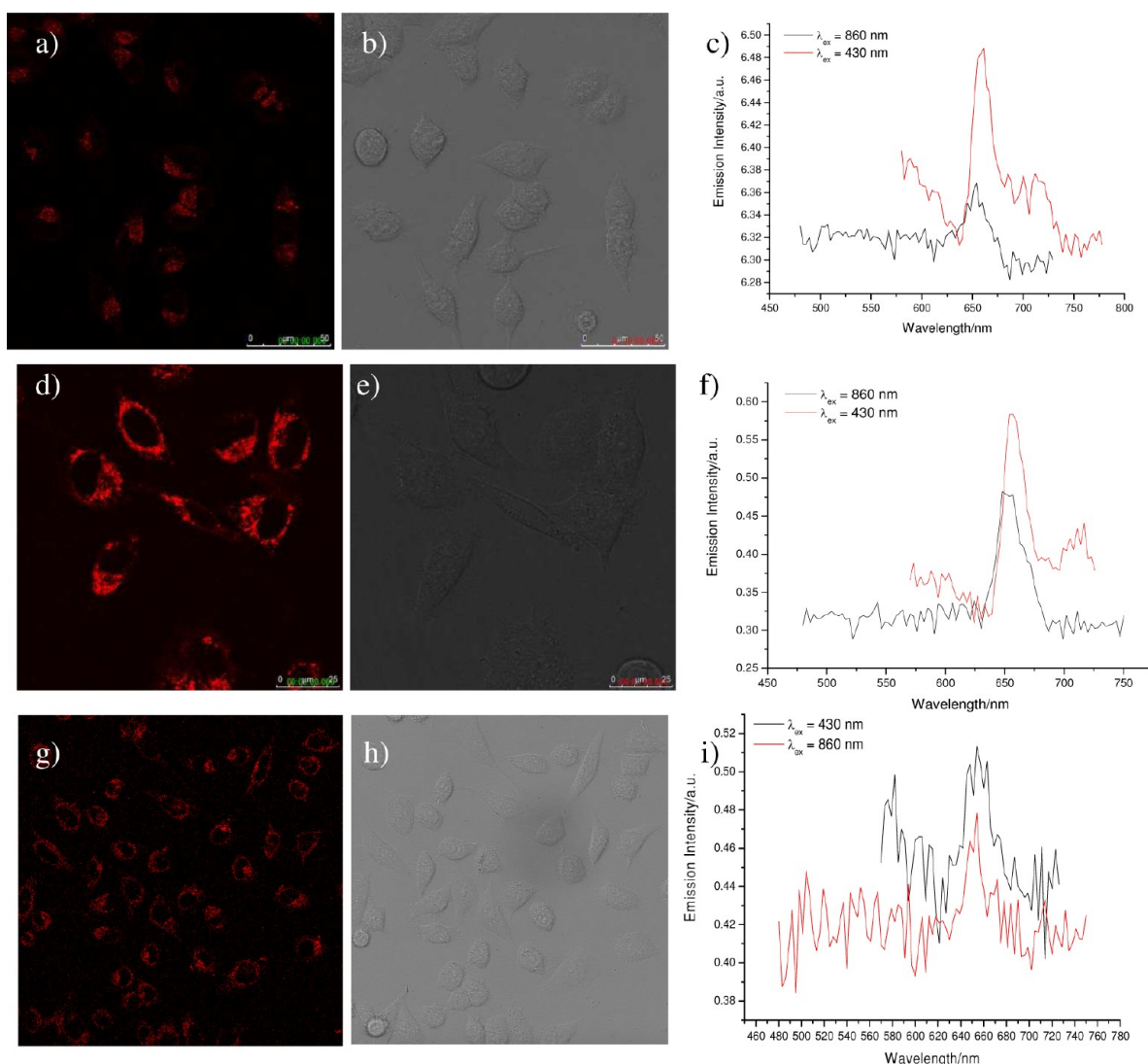


Figure 8. Confocal fluorescent microscopic images of the free-base porphyrin-Ru(II) conjugates **1** (a), **2** (d), and **3** (g) (dosed concentration = 2 μM , λ_{ex} = 860 nm, incubation time = 6 h), together with their corresponding bright-field images (**1** – b; **2** – e; **3** – h), linear (λ_{ex} = 430 nm) and two-photon induced (λ_{ex} = 860 nm) in vitro emission spectra in HeLa cells (resolution = 4 nm).

(Figure 8). Cells loaded with conjugates **1** (Figure 8a,b,c), **2** (Figure 8d,e,f), and **3** (Figure 8g,h,i) were excited by visible argon-ion (λ_{ex} = 432 nm, Figures S18 and S19) and near-infrared femtosecond lasers (λ_{ex} = 860 nm, Figure 8). The in vitro emission profiles of the three conjugates are similar under linear or two-photon excitation using the same dosed concentration and time duration.

The subcellular localizations of conjugates **1** and **2** were determined by costaining experiments using organelle-specific trackers. After 3 h of incubation, conjugate **1** showed specific localization in lysosomes (Figure S18), whereas conjugate **2** showed specific localization in mitochondria (Figure S19). Furthermore, when the in vitro luminescence of these conjugates was monitored hourly, 90% of the maximum luminescence (measured after 3 h) was observed after 2 h of incubation, showing a fairly rapid intracellular trafficking of these conjugates to their targeted organelles. As for conjugate **3**, it appeared to reside in the cytoplasm with no obvious organelle localization (Figure 8).

Dark Cytotoxicity and Photocytotoxicity. MTT assay was used to measure the cytotoxicity of conjugates **1**, **2**, and **3**.³⁷

The dose–response curves obtained by incubation of these conjugates in the dark at various concentrations ranging from 1 to 250 μM with HeLa cells are shown in Figure 9a. From these curves, the IC_{50} of **1**, **2**, and **3** were estimated to be 118, 175, and >250 μM , respectively. The lower cytotoxicity seen in **3** is presumably related to its lower cellular uptake rate by the cells.

The photocytotoxicity of conjugates **1**, **2**, and **3** was measured at 1 μM under varying light doses from 1.5 to 12.5 J/cm^2 . The light dose–response curves obtained are shown in Figure 9b. Conjugate **2** showed the strongest photocytotoxicity (LD_{50} = 2 J/cm^2), followed by conjugate **1** (LD_{50} = 6.5 J/cm^2), with conjugate **3** showing the weakest photocytotoxicity (LD_{50} = 11.5 J/cm^2) toward HeLa cells. This trend does not seem to correlate with either the cellular uptake rates of these conjugates (**1** ~ **2** \gg **3**) or their $^1\text{O}_2$ quantum yields (Table 1, **1** ~ **2** > **3**), but appears to correlate better with their subcellular localization properties. As **2** exhibits mitochondria-localizing property, its photoexcitation in this organelle produces $^1\text{O}_2$ -mediated oxidative stress which can readily elicit apoptotic cell death. Since **1** is shown to localize in lysosomes, its photoexcitation in this organelle produces $^1\text{O}_2$ that can

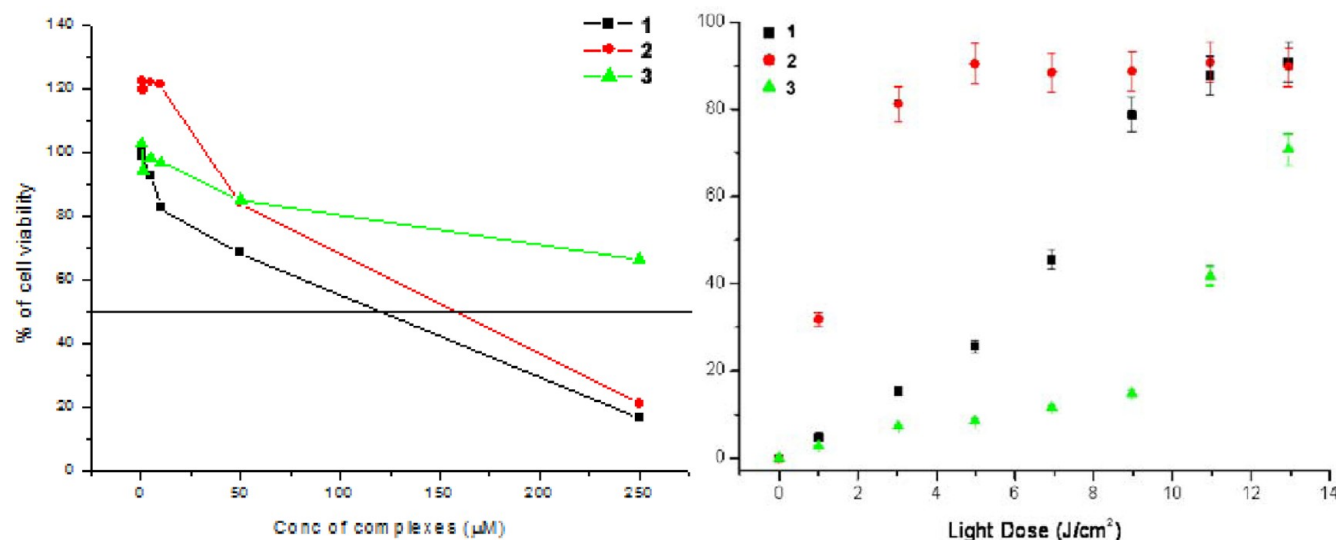


Figure 9. Dose–response curves of the dark cytotoxicity (left) and photocytotoxicity (right) of conjugates 1, 2, and 3. Dark cytotoxicity curves were obtained using dosed concentration from 1 to 250 μM . Photocytotoxicity curves were obtained using 1 μM of conjugates and various light doses from 0 to 12.5 J/cm^2 . MTT assay was carried out after incubation for 24 h. The results were expressed as the mean \pm SD of three separate trials.

Table 2. Summary of the in Vitro Properties of the Free-Base Porphyrin-Ru(II) Conjugates 1, 2, and 3

compound	cytotoxicity (IC_{50})		cellular uptake		subcellular localization	pK
	dark ^a (μM)	light ^b (J/cm^2)	flow cytometry ^c (1 h)	flow cytometry ^c (6 h)		
1	118	6.5	80-fold	500-fold	lysosome	3.75
2	175	2	80-fold	500-fold	mitochondria	3.26
3	>250	11.5	10-fold	20-fold	cytoplasm	4.39

^aDark cytotoxicities (IC_{50}) of 1, 2, and 3 toward HeLa cells were determined from the dose–response curve obtained after 24 h incubation with various concentrations of the conjugates. ^bPhotocytotoxicities of 1, 2, and 3 toward HeLa cells was determined using 1 μM of the conjugates under various light doses. MTT assay was performed on the HeLa cells after 24 h incubation. ^cThe luminescence signal measured (relative to the control) was used as the parameter for comparing the cellular uptake rates of the conjugates.

damage the lysosomal membrane, causing the release of the lysosomal enzymes which leads to necrosis. Conjugate 3, which is more hydrophilic, distributes in the cytoplasm. When photoexcited, 3 produces $^1\text{O}_2$ in the cytosol where a substantial $^1\text{O}_2$ population could become deactivated before inflicting damage on any vital subcellular targets to cause cell death. The results of the in vitro properties of these conjugates, 1–3, toward HeLa cells, which include their cellular uptake, subcellular localization, and dark cytotoxicity and photocytotoxicity, are summarized in Table 2.

Two-Photon Induced Imaging and Cytotoxicities of 1, 2, and 3. HeLa cells were incubated with 5 μM of conjugates 1, 2, or 3 separately for 6 h. The cells were then excited at 850 nm, at which the three conjugates 1, 2, and 3 showed a two-photon absorption cross section of 177, 168, and 144 GM, respectively. The confocal images were captured at one laser shot per minute for a total of 32 min. Figure 10 shows the confocal images of these cells after two-photon laser irradiation for time $t = 0, 8, 16,$ and 32 min. To demonstrate the potential use of conjugates 1, 2, and 3 as two-photon excited imaging agents, these conjugates stained HeLa cells were excited with a snap laser flash at 860 nm and the images were captured under a confocal microscope. A clear fluorescent image of the stained HeLa cells was obtained (Figure 10a,e,i). The fluorescence intensities of the 1- and 2-stained cells were greater than that of the 3-stained cells. This observation is consistent with the flow cytometric analysis (Figure 7) that the intracellular concentrations of 1 and 2 are greater than 3.

To further study the efficacy of these conjugates on two-photon induced cytotoxicity, the cells were continuously irradiated and the fluorescent images of the cells were captured at 8 (Figure 10b,f,j), 16 (Figure 10c,g,k), and 32 min (Figure 10d,h,l) after irradiation. After 2PA-PDT, the patterns of subcellular localization of conjugates 1 and 3 in the treated HeLa cells were similar to those of the control cells (Figure 10a,i). A significant nuclear localization of 2 (Figure 10f,g,h) was seen in cells at 8 to 32 min after irradiation. Cell shrinkage was also apparent at 16 to 32 min in the PDT-treated cells, indicating that conjugate 2-mediated PDT could effectively damage the nuclear membrane and caused the cell death. The nuclear localization of 2 is probably due to a redistribution of 2 from the cytoplasm (presumably released from the damaged mitochondria during initial PDT) to the nucleus. In this short-term cell imaging study, conjugate 2-mediated PDT is found to be more effective than 1 and 3 in triggering the cell death process. This result is also consistent with the result of conventional one-photon PDT-induced cell death assay as shown in Table 2.

CONCLUSION

Six water-soluble free-base porphyrin-Ru(II) conjugates, 1–3, and Zn(II) porphyrin-Ru(II) conjugates, 4–6, have been synthesized with satisfactory yields (>70%) and their potential development as dual in vitro imaging and photodynamic therapeutic agents investigated. Photoexcitation of conjugates 1–3 at 430 nm led to an energy transfer from the Ru(II)

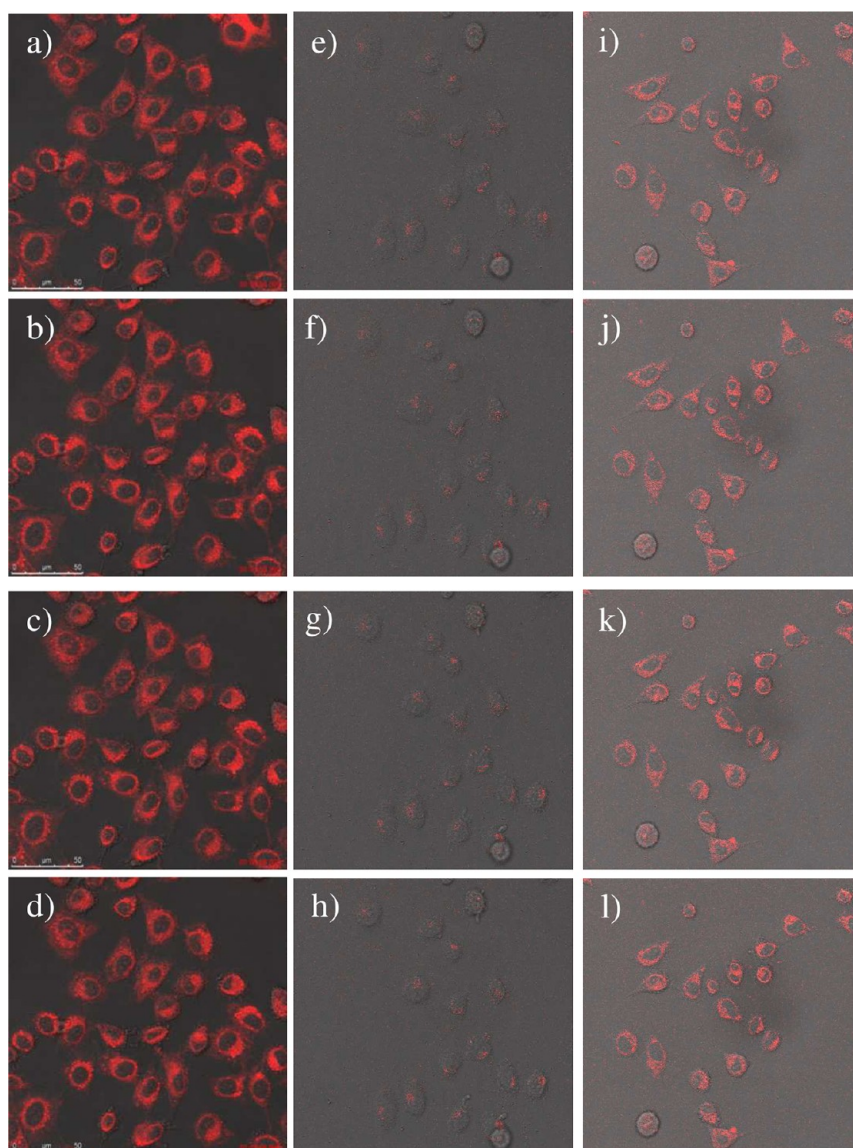


Figure 10. Confocal microscopic images of HeLa cells treated with $5 \mu\text{M}$ of **1** (a, b, c, d), **2** (e, f, g, h), and **3** (i, j, k, l) for 6 h. Top row: images obtained for **1** (left), **2** (middle), and **3** (right)-treated cells after one snap laser flash (to avoid $^1\text{O}_2$ generation) at 860 nm. Second row: images obtained after 8 min of laser irradiation. Third row: images obtained after 16 min of laser irradiation. Bottom row: images obtained after 32 min of laser irradiation.

$^1\text{MLCT}$ excited state to the porphyrin singlet state, resulting in emissions at ca. 659 and 718 nm. In contrast, photoexcitation of the Zn(II) porphyrin-Ru(II) conjugates, **4–6**, at 430 nm resulted in an energy transfer from the Soret-excited porphyrin to the Ru(II) due to an increase in the singlet energy level of Zn(II) porphyrin to above that of the Ru(II) $^3\text{MLCT}$ state. The emission quantum yields of these conjugates, **4–6**, were ca. 10-fold lower than those of conjugates **1–3**. An obvious dependence of the energy transfer efficiency on the linker of these conjugates was noted ($1 \sim 2 > 3$ and $4 > 5 > 6$), with the efficiency reduced by 2–3-fold via the longer ethoxyethane linkage. All conjugates gave $^1\text{O}_2$ quantum yields (ranging from 0.73 to 0.38) adequate for potential application as PDT agents, with no obvious difference between conjugates with different linkers. The two-photon absorption cross sections, σ^2 , of these conjugates ranged from 228 GM in **5** to 106 GM in **6**, with no expected enhancement from the “conjugative” phenylethynyl and phenylamide linkers. This observation is explained in terms

of the perpendicular orientation adopted by the phenyl-containing linkers which does not support the extension of the porphyrin π -conjugation to the polypyridyl ligand of the Ru(II) complex.

The in vitro properties of conjugates **1–3** toward HeLa cells were further investigated as they gave higher emission and $^1\text{O}_2$ quantum yields. The IC_{50} measured for conjugates **1**, **2**, and **3** in the dark were 118, 175, and $>250 \mu\text{M}$, which is consistent with their cellular uptake properties with $1 \sim 2 \gg 3$, where **3**, which contained a more hydrophilic poly(ethylene glycol) linkage, was the least efficient in cell penetration. The photocytotoxicity of these conjugates, however, gave the following light dose dependence at $1 \mu\text{M}$ concentration: **2** ($2 \text{ J}/\text{cm}^2$) $>$ **1** ($6.5 \text{ J}/\text{cm}^2$) $>$ **3** ($11.5 \text{ J}/\text{cm}^2$), which is explained by their respective subcellular localizations at the mitochondria, lysosomes and cytoplasm. These one-photon induced cytotoxicity data is consistent with the observed two-photon PDT data, which taken together strongly suggest the importance of

subcellular localization in affecting the in vitro PDT activity of a drug. Among the three porphyrin-Ru(II) conjugates studied, **2**, with its high emission quantum yield, low dark cytotoxicity, and high phototoxicity, is the most promising candidate for both in vitro imaging and PDT activity.

■ ASSOCIATED CONTENT

■ Supporting Information

Synthetic details, ^1H NMR spectra, HRMS spectra, $^1\text{O}_2$ phosphorescence spectra, comparative absorption and fluorescence spectra of the porphyrin-Ru(II) conjugates in free-base form (pH = 10.0) and dicationic form (pH = 2.0), luminescence decay curves of the six porphyrin-Ru(II) conjugates, costaining confocal microscopic images of **1** and **2**. This material is available free of charge via the Internet at <http://pubs.acs.org>.

■ AUTHOR INFORMATION

Corresponding Author

*E-mail: wk Wong@hkbu.edu.hk, kl Wong@hkbu.edu.hk, chiklau@cityu.edu.hk. Fax: +852-3411-5862. Tel: +852-34117011. Tel: +852-34112370.

Author Contributions

#The first to third authors contributed equally as co-1st author.

Notes

The authors declare no competing financial interest.

■ ACKNOWLEDGMENTS

The work described in this paper was partially supported by grants from the Research Grants Council of the Hong Kong SAR, P.R. China (HKBU 202509 and HKBU 202210) and a starting grant from the Hong Kong Baptist University (KLW).

■ ABBREVIATIONS:

PDT, photodynamic therapy; TPA, two-photon absorption; NIR, near-infrared; phen, 1,10-phenanthroline; bpy, 2,2'-bipyridine.

■ REFERENCES

- (1) Mack, J., and Kobayashi, N. (2011) Low symmetry phthalocyanines and their analogues. *Chem. Rev.* *111*, 281–321.
- (2) Biswas, S., Ahn, H.-Y., Bondar, M. V., and Belfield, K. D. (2011) Tetracene-doped anthracene nanowire arrays: preparation and doping effects. *Langmuir* *27*, 06374–06380.
- (3) Zhao, Z., Chan, P.-S., Li, H., Wong, K.-L., Wong, R. N. S., Mak, N.-K., Zhang, J., Tam, H.-L., Wong, W.-Y., Kwong, D. W. J., and Wong, W.-K. (2012) Highly selective mitochondria-targeting amphiphilic silicon (IV) phthalocyanines with axially ligated rhodamine B for photodynamic therapy. *Inorg. Chem.* *51*, 812–821.
- (4) Hasan, T., Ortel, B., Moor, A. C. E., and Pogue, B. W. (2003) *Holland-Frei Cancer Medicine* *6*, (Kufe, D. W., Pollock, R. E., Weichselbaum, R. R., Bast, R. C., Jr., Gansler, T. S., Holland, J. F., Frei, E., III, Eds.) pp 605–622, Decker, Hamilton.
- (5) Triesscheijn, M., Bass, P., Schellens, J. H. M., and Stewart, F. A. (2006) Photodynamic therapy in oncology. *The Oncologist* *11*, 1034–1044.
- (6) Brown, S. B., Brown, E. A., and Walker, I. (2004) The present and future role of photodynamic therapy in cancer treatment. *Lancet Oncol.* *5*, 497–508.
- (7) Dolmans, D. E. J. G. J., Fukumura, D., and Jain, R. K. (2003) Photodynamic therapy for cancer. *Nat. Rev. Cancer* *3*, 380–387.
- (8) Dougherty, T. J., Gomer, C. J., Henderson, B. W., Jori, G., Kessel, D., Korbek, M., Moan, J., and Peng, Q. (1998) Photodynamic therapy. *J. Natl. Cancer Inst.* *90*, 889–905.

- (9) Castano, A. P., Demidova, T. N., and Hamblin, M. R. (2004) Mechanisms in photodynamic therapy: part one—photosensitizers, photochemistry and cellular localization. *Photodiagn. Photodynam. Ther.* *1*, 279–293.

- (10) Castano, A. P., Demidova, T. N., and Hamblin, M. R. (2005) Mechanisms in photodynamic therapy: Part three-Photosensitizer pharmacokinetics, biodistribution, tumor localization and modes of tumor destruction. *Photodiagn. Photodynam. Ther.* *2*, 91–106.

- (11) Plaetzer, K., Krammer, B., Berlanda, J., Berr, F., and Klesslich, T. (2009) Photophysics and photochemistry of photodynamic therapy: fundamental aspects. *Lasers Med. Sci.* *24*, 259–268.

- (12) Detty, M. R., Gibson, S. L., and Wagner, S. J. (2004) Current clinical and preclinical photosensitizers for use in photodynamic therapy. *J. Med. Chem.* *47*, 3897–3915.

- (13) Moan, J. (1990) Properties for optimal PDT sensitizers. *J. Photochem. Photobiol. B: Biol.* *5*, 521–524.

- (14) MacDonald, I. J., and Dougherty, J. (2001) Basic principles of photodynamic therapy. *J. Porphyrins Phthalocyanines* *5*, 105–129.

- (15) Vicente, M. G. (2001) Porphyrin-based sensitizers in the detection and treatment of cancer: recent progress. *Curr. Med. Chem.: Anti-cancer Agents* *2*, 175–194.

- (16) Schmitt, F., Govindaswamy, P., Süß-Fink, G., Ang, W. H., Dyson, P. J., Juillerat-Jeanneret, L., and Therrien, B. (2008) Ruthenium porphyrin compounds for photodynamic therapy of cancer. *J. Med. Chem.* *51*, 1811–1816.

- (17) Bergamo, A., Gaiddon, C., Schellens, J. H. M., Beijnen, J. H., and Sava, G. (2011) Approaching tumour therapy beyond platinum drugs: status of the art and perspectives of ruthenium drug candidates. *J. Inorg. Biochem.* *106*, 90–99.

- (18) Ang, W. H., Casini, A., Sava, G., and Dyson, P. J. (2011) Organometallic ruthenium-based antitumor compounds with novel modes of action. *J. Organomet. Chem.* *696*, 989–998.

- (19) Antonarakis, E. S., and Emadi, A. (2010) Ruthenium-based chemotherapeutics: are they ready for prime time? *Cancer Chemother. Pharmacol.* *66*, 1–9.

- (20) Suess-Fink, G. (2010) Arene ruthenium complexes as anticancer agents. *Dalton Trans.* *39*, 1673–1688.

- (21) Bruijninx, P. C. A., and Sadler, P. J. (2009) Controlling platinum, ruthenium, and osmium reactivity for anticancer drug design. *Adv. Inorg. Chem.* *61*, 1–62.

- (22) Gianferrara, T., Bergamo, A., Bratsos, I., Milani, B., Spagnol, C., Sava, G., and Alessio, E. (2010) Ruthenium–porphyrin conjugates with cytotoxic and phototoxic antitumor activity. *J. Med. Chem.* *53*, 4678–4690.

- (23) Juzeniene, A., Peng, Q., and Moan, J. (2007) Milestones in the development of photodynamic therapy and fluorescence diagnosis. *Photochem. Photobiol. Sci.* *6*, 1234–1245.

- (24) Moan, J. J. (1990) On the diffusion length of singlet oxygen in cells and tissues. *Photochem. Photobiol. B: Biol.* *6*, 343–344.

- (25) Poon, C. T., Chan, P. S., Man, C., Jiang, F.-L., Wong, R. N. S., Mak, N. K., Kwong, D. W. J., Tsao, S. W., and Wong, W. K. (2010) An amphiphilic ruthenium(II)-polypyridyl appended porphyrin as potential bifunctional two-photon tumor-imaging and photodynamic therapeutic agent. *J. Inorg. Biochem.* *104*, 62–70.

- (26) Ke, H.-Z., Wang, H.-D., Wong, W. K., Mak, N. K., Kwong, D. W. J., Wong, K.-L., and Tam, H.-L. (2010) Responsive and mitochondria-specific ruthenium(II) complex for dual in vitro applications: two-photon (near-infrared) induced imaging and regioselective cell killing. *Chem. Commun.* *46*, 6678–6680.

- (27) Saha, S., Mallick, D., Majumdar, R., Roy, M. R., Dighe, R. D., Jemmis, E. R., and Chakravarty, A. (2011) Structure–activity relationship of photocytotoxic iron(III) complexes of modified dipyrrolophenazine ligands. *Inorg. Chem.* *250*, 2975–2987.

- (28) Sullivan, B. P., Salmon, D. J., and Meyer, T. J. (1978) Mixed phosphine 2,2'-bipyridine complexes of ruthenium. *Inorg. Chem.* *17*, 3334–3341.

- (29) Ziessel, R. (1996) General method for the preparation of alkyne-functionalized oligopyridine building blocks. *J. Org. Chem.* *61*, 6535–6546.

- (30) Faragher, R. J., and Schwan, A. L. (2008) New deuterated oligo(ethylene glycol) building blocks and their use in the preparation of surface active lipids possessing labeled hydrophilic tethers. *J. Org. Chem.* 73, 1371–1378.
- (31) heik-Bahae, M., Said, A. A., Wei, T.-H., Hagan, D. J., and Van Stryland, E. W. (1990) Sensitive measurement of optical nonlinearities. *IEEE J. Quantum Electron.* 26, 760–769.
- (32) Zhang, J., Wong, K.-L., Wong, W.-K., Mak, N.-K., Kwong, W. J. D., and Tam, H. L. (2011) Two-photon induced luminescence, singlet oxygen generation, cellular uptake and photocytotoxic properties of amphiphilic Ru(II) polypyridyl-porphyrin conjugates as potential bifunctional photodynamic therapeutic agents. *Org. Biomol. Chem.* 50, 5517–5525.
- (33) Li, Y., Pritchett, T. M., Huang, J., Ke, M., Shao, P., and Sun, W. (2008) Photophysics and nonlinear absorption of peripheral-substituted zinc phthalocyanines. *J. Phys. Chem. A* 112, 7200–7207.
- (34) Mak, N. K., Li, K. M., Leung, W. N., Wong, R. N., Huang, D. P., Lung, M. L., Lau, Y. K., and Chang, C. K. (2004) Involvement of both endoplasmic reticulum and mitochondria in photokilling of nasopharyngeal carcinoma cells by the photosensitizer Zn-BC-AM. *Biochem. Pharmacol.* 68, 2387–2396.
- (35) Gouterman, M. (1978) *The Porphyrins: Physical Chemistry* (Dolphin, D., Ed.) p 1, Vol. III, Academic Press, New York.
- (36) Lee, W. A., Graetzel, M., and Kalyanasundaram, K. (1984) Anomalous ortho effects in sterically hindered porphyrins: tetrakis(2,6-dimethylphenyl)porphyrin and its sulfonate derivative. *Chem. Phys. Lett.* 107, 308–313.
- (37) Kon, H., Tsuge, K., Imamura, T., Sasaki, Y., Ishizaka, S., Kitamura, N., and Kato, M. (2008) Excitation energy flow control in {Ru(2,2'-bipyridine)₂}-{pyridylporphyrin}₂ systems. *Dalton Trans.* 12, 1541–1543.
- (38) Flamigni, L. (2001) Charge separation and energy transfer in multicomponent porphyrinic arrays. *Pure Appl. Chem.* 3, 421–424.
- (39) Flamigni, L., Armaroli, N., Barigelletti, F., Balzani, V., Collin, J.-P., Dalbavie, J.-O., Heitz, V., and Sauvage, J.-P. (1997) Photoinduced processes in dyads made of a porphyrin unit and a ruthenium complex. *J. Phys. Chem. B* 101, 5936–5943.
- (40) Collin, J.-P., Harriman, A., Heitz, V., Odobel, F., and Sauvage, J.-P. (1994) Photoinduced electron- and energy-transfer processes occurring within porphyrin-metal-bisterpyridyl conjugates. *J. Am. Chem. Soc.* 116, 5679–5690.
- (41) Albertazzi, L., Storti, B., Marchetti, L., and Beltram, F. (2010) Delivery and subcellular targeting of dendrimer-based fluorescent pH sensors in living cells. *J. Am. Chem. Soc.* 132, 18158–18167.
- (42) Wu, M. M., Llopis, J., Adams, S., McCaffery, J. M., Kulomaa, S. M., Machen, T. E., Moore, H.-P. H., and Tsien, R. Y. (2000) Organelle pH studies using targeted avidin and fluorescein-biotin. *Chem. Biol.* 3, 197–209.
- (43) Ohkuma, S., and Poole, B. (1978) Fluorescence probe measurement of the intralysosomal pH in living cells and the perturbation of pH by various agents. *Proc. Natl. Acad. Sci. U.S.A.* 75, 3327–3331.
- (44) Abiko, A., and Masamune, S. (1996) Synthesis of (+)-siphonarienone: Asymmetric alkylation using a chiral benzopyranoisoxazolidine auxiliary. *Tetrahedron Lett.* 37, 1081–1084.
- (45) Han, J., and Burgess, K. (2010) Fluorescent indicators for intracellular pH. *Chem. Rev.* 110, 2709–2728.
- (46) Paroutis, P., Touret, N., and Grinstein, S. (2004) The pH of the secretory pathway: measurement, determinants, and regulation. *Physiology* 19, 207–215.
- (47) Orij, R., Postmus, J., Ter Beek, A., Brul, S., and Smits, G. J. (2009) In vivo measurement of cytosolic and mitochondrial pH using a pH-sensitive GFP derivative in *Saccharomyces cerevisiae* reveals a relation between intracellular pH and growth. *Microbiology* 155, 268–278.
- (48) Bagar, T., Altenbach, K., Read, N. D., and Benčina, M. (2009) Live-cell imaging and measurement of intracellular pH in filamentous fungi using a genetically encoded ratiometric probe. *Eukaryotic Cell* 5, 703–712.
- (49) Hambright, P. (2000) Chemistry of water soluble porphyrins. In *The Porphyrin Handbook* (Kadish, K. M., Smith, K. M., and Guillard, R., Eds.) Chapter 18, Academic Press, New York.
- (50) Finikova, O. S., Cheprakov, A. V., Carroll, P. J., Dalosto, S., and Vinogradov, S. A. (2002) Influence of nonplanarity and extended conjugation on porphyrin basicity. *Inorg. Chem.* 41, 6944–6946.
- (51) Barkigia, K. M., Berber, M. D., Fajer, J., Medforth, C. J., Renner, M. W., and Smith, K. M. (1990) Nonplanar porphyrins. X-ray structures of (2,3,7,8,12,13,17,18-octaethyl- and -octamethyl-5,10,15,20-tetraphenylporphinato)zinc(II). *J. Am. Chem. Soc.* 112, 8851–8857.
- (52) Takeda, J., Ohya, T., and Sato, M. (1992) A ferrochelatase transition-state model. Rapid incorporation of copper (II) into nonplanar dodecaphenylporphyrin. *Inorg. Chem.* 31, 2877–2880.
- (53) Vinogradov, S. A., and Wilson, D. F. (2000) Electrostatic core shielding in dendritic polyglutamic porphyrins. *Chem.-Eur. J.* 6, 2456–2461.
- (54) Kohata, K., Higashio, H., Yamaguchi, Y., Koketsu, M., and Odashima, T. (1994) Synthesis and characterization of new style of water-soluble glycosylated porphyrins as a spectrophotometric reagent for metal ions. *Bull. Chem. Soc. Jpn.* 67, 668–679.
- (55) Finikova, O., Galkin, A., Rozhkov, V., Cordero, M., Hägerhäll, C., and Vinogradov, S. (2003) Porphyrin and tetrabenzoporphyrin dendrimers: tunable membrane-impermeable fluorescent pH nano-sensors. *J. Am. Chem. Soc.* 125, 4882–4893.
- (56) Valiotti, A., Adeyemo, A., Williams, R. F. X., Ricks, L., North, J., and Hambright, P. (1981) A water soluble “picket fence” porphyrin and its isomers. *J. Inorg. Nucl. Chem.* 43, 2653–2658.
- (57) Tan, L.-S., Zheng, Q., and Prasad, P. N. (2008) Multiphoton absorbing materials: molecular designs, characterizations, and applications. *Chem. Rev.* 108, 1245–1330.
- (58) Maiti, M., and Steer, R. P. (2009) Soret-excited ZnTPP quenched by electron transfer in chlorinated solvents? *Chem. Phys. Lett.* 482, 254–258.
- (59) Zhang, J. X., Wong, K. L., Wong, W. K., Mak, N. K., Kwong, D. W. J., and Tam, H. L. (2011) Two-photon induced luminescence, singlet oxygen generation, cellular uptake and photocytotoxic properties of amphiphilic Ru(II) polypyridyl-porphyrin conjugates as potential bifunctional photodynamic therapeutic agents. *Org. Biomol. Chem.* 9, 6004–6010.
- (60) Puckett, C. A., and Barton, J. K. (2007) Methods to explore cellular uptake of ruthenium complexes. *J. Am. Chem. Soc.* 129, 46–47.
- (61) Gasser, G., Ott, I., and Metzler-Nolte, N. (2011) Organometallic anticancer compounds. *J. Med. Chem.* 54, 3–25.
- (62) Gianferrara, T., Bratsos, I., Iengo, E., Milani, B., Oštrić, A., Spagnol, C., Zangrando, E., and Alessio, E. (2009) Synthetic strategies towards ruthenium-porphyrin conjugates for anticancer activity. *Dalton Trans.* 48, 10742–10756.
- (63) Puckett, C. A., and Barton, J. K. (2008) Mechanism of cellular uptake of a ruthenium polypyridyl complex. *Biochemistry* 47, 11711–11716.